# Supporting Information

## Geometric Orthogonality as a Recipe for Efficient Intramolecular Charge Generation in Core Substituted NDI Derivatives

Hugh C. Britton,*[a,b]‡ Alberto M. Santa Daría,[c]‡ Chao Lyu,[b]‡ Andras B. Augusztin,[b] Lewis M. Cowen,[b] Dejan-Krešimir Bučar,[b] Alethea B. Tabor,[b] Bob C. Schroeder,[b] Sandra Gómez*[c,d] and Jose M. Marin-Beloqui*[e,f]

a Dr. Hugh C. Britton
School of Chemistry and Chemical Engineering,
University of Southampton
Southampton, London, UK, SO17 1BJ
E-mail: H.C.Britton@soton.ac.uk

b Dr. Hugh C. Britton, Chao Lyu, Andras B. Augusztin, Dr. Lewis M. Cowen, Dr. Dejan-Krešimir Bučar, Prof Alethea B. Tabor, Prof Bob C. Schroeder
Department of Chemistry
University College London, London, UK

c Dr. Alberto Martín Santa Daría, Dr. Sandra Gómez
Department of Physical Chemistry
Universidad de Salamanca
Pl. de los Caídos s/n, 37008 Salamanca (Spain)
E-mail: sandra.gomez@usal.es

d Dr. Sandra Gómez
Department of Chemistry
Universidad Autónoma de Madrid
C. Francisco Tomás y Valiente, 7, Fuencarral-El Pardo, 28049 Madrid
E-mail: sandra.gomezr@uam.es

e Dr. Jose M. Marin-Beloqui
Department of Physical Chemistry
University of Malaga
Andalucia-Tech Campus de Teatinos s/n, 29071 Málaga (Spain)

f Dr. Jose M. Marin-Beloqui
Materials and Nanotechnology College Institute (IMANA)
University of Malaga
Campus de Teatinos s/n, 29071 Málaga (Spain)
E-mail: jm.marinbeloqui@uma.es

‡ These authors contributed equally to this work

Supporting information for this article is given via a link at the end of the document.

## Summary

# 1. Experimental Section

## Synthesis

Common solvents and chemicals for organic synthesis were purchased from Sigma-Aldrich (Merck), Tokyo Chemical Industry, Fluorochem, VWR, Manchester Organics and Fisher Scientific and used as received. All anhydrous solvents were purchased and used as supplied.

All water used in experiments, synthesis and purification was Milli-Q grade water.. Deuterated solvents were purchased from Sigma-Aldrich (Merck). Air sensitive reactions were carried out under inert Ar atmosphere using standard Schlenk techniques.

Microwave synthesis was carried out in an *Anton-Paar Monowave 400* microwave reactor. Thin layer chromatography (TLC) was performed using Merck Si60 $F_{254}$ aluminium sheets and flash column chromatography was performed using Merck Geduran Si60 silica gel (40-63 μm particle size).

$^{1}H$ and $^{13}C$ nuclear magnetic resonance (NMR) spectra were recorded on Bruker NMR spectrometers *Avance Neo 500*, *Avance III 600* and *Avance Neo 700* at 298 K. Chemical shifts (δ) are reported as parts per million (ppm) using residual solvent peak as internal standards. Coupling constants (*J*) are given in Hertz (Hz) and spin multiplicities denoted as follows: s = singlet, d = doublet, t = triplet, q = quartet, quint = quintet, br = broad signal, m = multiplet. Mass spectrometry (MS) data were collected on a *Thermo Scientific Exactive Plus Orbitrap* (ASAP-MS, HRMS-ESI), *Waters Micromass MALDI micro MX* (MALDI-TOF), and *Waters Acquity UPLC* with UV detector connected to *Waters Acquity SQD* (LCMS) mass spectrometers. Fourier-transform infrared spectroscopy (FTIR) was performed using a *Bruker ALPHA* FTIR spectrometer on solid samples. Melting points were measured on an *Electrothermal IA9300* melting point apparatus. Kugelrohr distillation was performed using a Buchi B-585 glass oven.

**General Method 1: Microwave Stille coupling of aryl-tributyl stannanes and NDI-anhydride $Br_2$NDA** [1,2]

To an oven dried 30 mL microwave vial under argon was added 2,6-dibromo-1,4,5,8-naphthalenetetracarboxylic dianhydride **$Br_2$NDA** (0.50 g, 1.174 mmol, 1.0 eq), tri-*n*-butylarylstannane (2.5 eq), rinsed in with PhCl (8 mL). The vial was sealed under Ar and sparged with Ar from a balloon while sonicated, for 25 min. To this homogenised mixture was added $PdCl_2(PPh_3)_2$ (0.1 eq) and the suspension heated under microwave conditions (600 rpm, ramp RT-180°C over 5 min, held at 180 °C for 20 min). After cooling to RT, the resulting suspension was filtered, and the solid reslurried in MeOH (20 mL, 10 min) then $CHCl_3$ (20 mL, 10 min). Filtration and drying resulted in the crude intermediate as a strongly coloured solid.

**General Method 2: Thermal (Sealed Tube) imide formation with β-alanine** [3,4]

2,6-Substituted-1,4,5,8-naphthalenetetracarboxylic dianhydride **1a-e** (1 eq), was mixed with β-alanine (3 - 4 eq) in glacial AcOH (10 vol) in a sealed flask. The mixture was then sonicated for 10 min then immersed in a silicon oil bath (120-140 °C) and monitored by $^{1}H$ NMR until complete consumption of the starting material (observed by a slight change in the chemical shift of the naphthalene core C-H from anhydride to imide). The reaction was then cooled to

RTnd the coloured precipitate was filtered, washed with glacial AcOH (3 x 30 mL), and dried under vacuum overnight to give the isolated product.

**General Method 3: Single crystal growth for X-ray diffraction**

**NDI-Ph**, **NDI-Th** and **NDI-An** crystals were obtained by a diffusion method using tetrahydrofuran and diethyl ether. The same method was also used for further purification of these compounds to obtain high quality NMR spectra. First, the target NDI was dissolved as much as possible in tetrahydrofuran, using heating and sonication to obtain a saturated or nearly saturated solution. Then, the undissolved particles were removed via a syringe filter to obtain a clear solution, which was transferred into a clean small vial afterwards. In a larger sample vial, an appropriate amount of diethyl ether was added as antisolvent with the small vial inside and lid sealed. Over time, the antisolvent, which diffuses more easily, gradually transferred into inner vial, reducing the solubility of the target NDI in the mixed solvent and leading to crystallisation.

## Single crystal X-ray diffraction measurements

The diffraction data for **NDI-Th**, **NDI-Ph** and **NDI-An** were collected on a four-circle *Agilent SuperNova* (Dual Source) single crystal X-ray diffractometer using a micro-focus Cu$K_\alpha$ X-ray beam ($\lambda$ = 1.54184 Å) and a *HyPix-Arc 100°* hybrid pixel array detector. The sample temperatures were controlled with an *Oxford Instruments* cryojet. All data were processed using the *CrysAlis$^{Pro}$* software.[5]

The crystal structures were solved with the *SHELXT* programme,[6] used within the *Olex2* software suite,[7] and refined by least squares on the basis of $F^2$ with the *SHELXL*[8] programme using the *ShelXle* graphical user interface.[9] All non-hydrogen atoms were refined anisotropically by the full-matrix least-squares method. Hydrogen atoms associated with carbon atoms were refined isotropically [$U_{iso}$(H) = 1.2$U_{eq}$(C)] in geometrically constrained positions.

**Crystal structure refinement details**

The crystal structure of **NDI-Th** features a disordered thiophene group and a THF molecule. Their geometries were restrained and/or constrained using the DANG, DFIX, FLAT, EXYZ, EADP and SAME commands in SHELXL.

The data for the **NDI-An** diethyl ether solvate was collected at 100 K to reduce the disorder of diethyl ether in its structure. The disordered solvent molecule was identified as diethyl ether based on the positions of residual electron density peaks in the difference Fourier map and an calculation of the bulk-solvent contribution to the calculated structure factors using the Solvent Masking routine in *Olex2*.[10] This analysis revealed a total of 41 electrons in a volume of 138 Å$^3$ in the asymmetric unit, which is consistent with the presence of two diethyl ether (84 electrons) per formula unit. Based on these findings, the solvated structure was refined using the DANG, DFIX, EADP, ISOR, SAME and SUMP commands in SHELXL.

The structure of the **NDI-An** diethyl-ether THF solvate hosts highly disordered solvent molecules that could not be adequately modelled. A data collection at 100 K was not feasible owing to persisting icing of the loop during data collection and the required long data collection time. In addition, the single crystal desolvated rapidly (as evidenced by the immediate

appearance of bubbles around the crystal as soon it is submerged in oil), leaving no opportunity to analyse a fully solvated crystal. The disordered solvent molecules were identified as diethyl ether and THF based on the positions of residual electron density peaks in the difference Fourier map, and an calculation of the bulk-solvent contribution to the calculated structure factors, using the Solvent Masking routine in *Olex2*.[10] This analysis suggested that the asymmetric contains a third of a diethyl ether molecule (22 electrons) in a 75 $Å^3$ void, and one and a half THF molecules (62 electrons) a 263 $Å^3$ void. The crystal structure was finally refined using the Solvent Masking routine.

Relevant crystallographic information and refinement parameters are shown in **Table S4**. The refinement details for each structure are described in Section 6 Crystallographic data, Figures S15 to S18.

## Spectroscopic characterisation

Absorbance was measured with an Agilent 8453 spectrophotometer. Emission properties were evaluated using a spectrofluorometer from Edinburgh Analytical Instrument (FLS920P) equipped with a pulsed xenon flash-lamp, Xe900, of 400 mW. Femtosecond transient absorption spectroscopy characterisation has been carried out with an Ultrafast Systems Helios. This equipment includes an amplified femtosecond Spectra-Physics Solstice-100F laser with a 128 fs pulse width and 1 KHz repetition rate. This laser is coupled with a Spectra-Physics TOPAS Prime F optical parametric amplifier (195-22000 nm). Samples were studied in 2-MeTHF solutions.

## Electrochemical characterisation

Cyclic voltammetry (CV) experiments were performed in a three-electrode system using a glassy carbon working electrode, a platinum wire as counter electrode, and a $Ag/AgNO_3$ (0.01 M in acetonitrile) reference electrode. The electrolyte solution consisted of 0.1 M tetrabutylammonium hexafluorophosphate ($TBAPF_6$) in DMF, containing 1mM of tested NDI. The potential was scanned from +0.1 V to –1.5 V vs. $Ag/AgNO_3$ at a scan rate of 0.1 V/s. Each measurement involved five consecutive cycles. All experiments were conducted after purged with nitrogen to exclude oxygen, and ferrocene was used as the reference for potential calibration (scanned from -0.2 V to +0.9 V).

## 2. Synthesis

**2,6-Dibromo-1,4,5,8-naphthalenetetracarboxylic dianhydride $Br_2NDA$** [11]

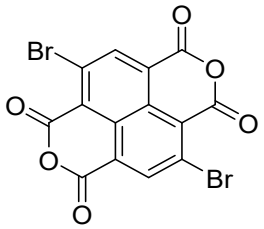

**$Br_2NDA$**

Naphthalene-1,3,6,8-tetracarboxylic acid anhydride (3.00 g, 11.3 mmol) was charged to a 250 mL glass pressure vessel containing a large stirrer bar, followed by neat sulfuric acid (25 mL). The stirred suspension was heated to 70 °C until full dissolution of the solids, then 1,3-dibromo-5,5-dimethylhydantoin (6.44 g, 22.6 mL) was added in one portion and the vessel directly sealed. The vessel was heated to 100 °C for 16 h then the contents carefully poured onto ice (*ca* 500 g). The resulting yellow solid was filtered, washed with cold water (2 x 50 mL) and MeOH (2 x 50 mL) and dried to give the known title compound (3.78 g, 78.7%) as a mixture of isomers which was carried forward to the next step without purification. Molar ratio of isomers: 49.1:9.7:8.0:1.6:1.0 of *trans-di*-Br: *tri*-Br: *mono*-Br: *cis-di*-Br: SM; w/w purity of *trans-di*-Br of 70.4%. NMR data of the major isomer was identical to the literature:[4] $^1$H NMR (500 MHz, DMSO-$d_6$) δ 8.79 (2H, s, Ar*H*); $^{13}$C NMR (125 MHz, DMSO-$d_6$) δ 158.0, 156.5, 137.6, 129.4, 127.5, 124.3, 123.4); IR $\nu_{max}$ 3082, 1781, 1742, 1566 cm$^{-1}$; *m/z* (ASAP-MS, ESI+) calcd for $C_{14}H_2O_6Br_2$ $[M+H]^+$ 424.8291; found 424.8296.

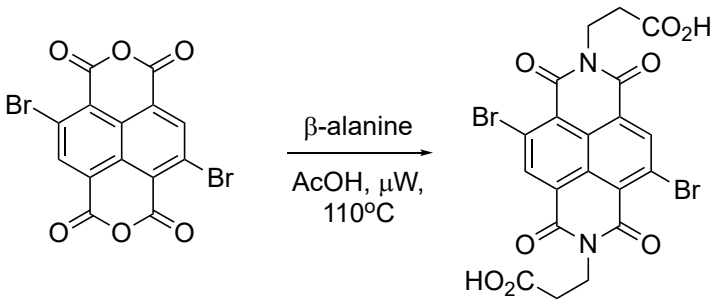


**$Br_2NDA$** **$Ala_2NDI$**

**Scheme S1** Conversion of **$Br_2NDA$** to **$Ala_2NDI$**

**3,3'-(4,9-dibromo-1,3,6,8-tetraoxo-1,3,6,8-tetrahydrobenzo[lmn][3,8] phenanthroline-2,7-diyl)dipropionic acid $Ala_2NDI$** [12]

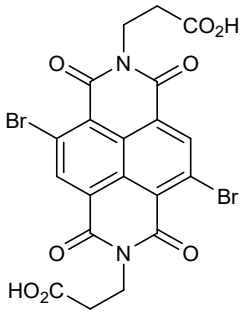


**$Ala_2NDI$**

2,6-Dibromo-1,4,5,8-naphthalenetetracarboxylic dianhydride **$Br_2NDA$** (0.899 g, 2.11 mmol), was mixed with β-alanine (0.7041 g, 7.90 mmol, 4 eq) in glacial AcOH (10 mL) in a sealed 30 mL microwave vial. The mixture was then sonicated for 10 min. The solution was heated to 110 °C over 5 min in a microwave reactor, then was kept at a steady temperature for 20 min. The reaction was then cooled to 55 °C before the vial was removed from the microwave. The coloured precipitate was filtered, washed with glacial AcOH (3 x 30 mL), and dried under vacuum overnight to give the isolated product as a bright orange solid (0.865 g, 72%). mp: 282-283 °C decomp.; $^1$H NMR (600 MHz, DMSO-$d_6$) δ 12.41 (2H, br s, $CO_2H$), 8.64-7.75 (2H, m, ArH), 4.22-4.29 (4H, m, $NCH_2$), 2.59-2.64 (4H, m, $CH_2CO_2H$); IR $\nu_{max}$ ($cm^{-1}$) 3055, 2923, 1691, 1654, 1560; m/z (ASAP-MS, ESI+) calcd for $C_{20}H_{12}N_2O_8Br_2$ $[M+H]^+$ 566.9033; found 566.9039.

**4,9-diphenylisochromeno[6,5,4-def]isochromene-1,3,6,8-tetraone 1°** [2]

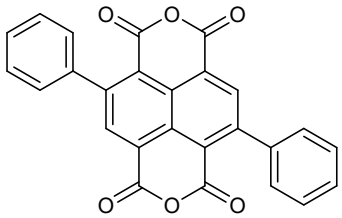


**1a**

2,6-Dibromo-1,4,5,8-naphthalenetetracarboxylic dianhydride **$Br_2NDA$** (1.20 g, 2.82 mmol, 1.0 eq) and tri-n-butylphenylstannane (2.3 mL, 7.04 mmol, 2.5 eq) in PhCl (19 mL) in the presence of $PdCl_2(PPh_3)_2$ (198 mg, 0.282 mmol, 0.1 eq) were reacted according to **General Method 1** to give the desired product **1a** as a yellow solid (0.693 g, 58% - 90% wrt the % of trans dibromide in the **$Br_2NDA$** starting material). IR $\nu_{max}$ ($cm^{-1}$) 3066, 1771, 1740, 1587, 1415; H NMR (500 MHz, DMSO) δ 8.43 (s, 2H, ArH), 7.61 – 7.51 (m, 10H, ArH); $^{13}$C NMR (126 MHz, DMSO) δ 159.47, 157.75, 146.70, 138.96, 135.05, 128.88, 128.72, 128.66, 128.44, 123.94, 121.36; m/z (ASAP-MS, ESI+) calcd for $C_{26}H_{13}O_6$; $[M+H]^+$ 421.0707; found 421.0708.

**Tributyl(mesityl)stannane** [13]

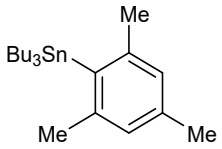


To a commercially available solution of mesityl magnesium bromide (1 M in THF, 20 mL, 20 mmol) under an Ar atmosphere at -78°C, was added tri-*n*-butyltin chloride (5.45 mL, 15 mmol, 1.0eq) dropwise. Precipitation of solids impeded stirring therefore THF (20 mL) was added. The resulting suspension was stirred for 1 h at -78 °C then returned to room temperature and stirred overnight. After concentration, the residue was purified by Kugelrohr distillation (up to 195 °C, 0.2 Torr) to give the title product (7.972 g, 97%) as a clear oil; $^{1}$H NMR (500 MHz, $CDCl_3$) δ 6.87 (s, 2H), 2.40 (s, 6H), 2.30 (s, 3H), 1.59 – 1.50 (m, 6H), 1.42 – 1.32 (m, 6H), 1.12 (app. t, *J* = 8.4 Hz, 6H).0.93 (t, J = 7.3 Hz, 9H); $^{13}$C NMR (126 MHz, $CDCl_3$) δ 145.4, 138.5, 138.0, 127.8, 29.4, 27.6, 25.7, 21.1, 13.8, 12.7.

***4,9-dimesitylisochromeno[6,5,4-def]isochromene-1,3,6,8-tetraone* 1b**

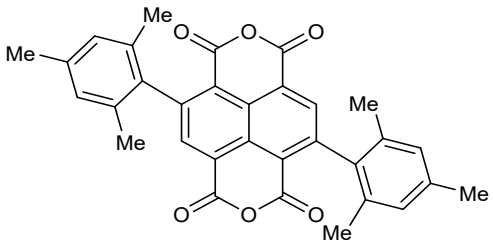


**1b**

2,6-Dibromo-1,4,5,8-naphthalenetetracarboxylic dianhydride **$Br_2$NDA** (0.750 g, 1.76 mmol, 1.0 eq) and tributyl(mesityl)stannane[12] (2.16 g, 5.28 mmol, 3.0 eq) in PhCl (12 mL) in the presence of $PdCl_2(PPh_3)_2$ (123 mg, 0.175 mmol, 0.1 eq) were reacted according to **General Method 1** to give the desired product **1b** as a green solid (0.4711 g, 53%). $^{1}$H NMR (500 MHz, DMSO) δ 8.20 (s, 2H), 7.01 (s, 4H), 2.34 (s, 6H), 1.90 (s, 12H); $^{13}$C NMR (126 MHz, DMSO) δ 159.6, 157.2, 146.4, 136.8, 136.0, 134.4, 133.8, 130.3, 129.1, 128.4, 128.2, 125.0, 122.1, 20.8, 20.2; IR $\nu_{max}$ ($cm^{-1}$) 2966, 2917, 1716, 1748, 1612, 1582, 1408; m/z (ASAP-MS, ESI+) calcd for $C_{32}H_{24}O_6$ [M+H$^+$]: 505.1646; found: 505.1644.

**4,9-di(thiophen-2-yl)isochromeno[6,5,4-def]isochromene-1,3,6,8-tetraone 1c** [14]

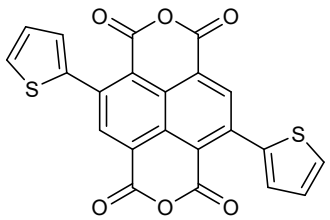


**1c**

2,6-Dibromo-1,4,5,8-naphthalenetetracarboxylic dianhydride **$Br_2$NDA** (1.00 g, 2.34 mmol, 1.0 eq) and tri-n-butyl(thiophen-2-yl)stannane (1.86 mL, 5.87 mmol, 2.5 eq) in PhCl (20 mL) in the presence of $PdCl_2(PPh_3)_2$ (164 mg, 0.234 mmol, 0.1 eq) were reacted according to **General**

**Method 1** to give the desired product **1c** as a dark red solid (0.5133 g, 51% (78% wrt the % of trans dibromide in the **$Br_2$NDA** starting material).

$^1$H NMR (500 MHz, DMSO) δ 8.50 (s, 2H, ArH), 7.90 (dd, *J* = 5.1, 1.2 Hz, 2H), 7.57 (dd, *J* = 3.6, 1.2 Hz, 2H), 7.27 (dd, *J* = 5.1, 3.6 Hz, 2H); $^{13}$C NMR (126 MHz, DMSO) δ 159.2, 157.6, 139.3, 138.7, 135.5, 130.2, 129.9, 129.1, 127.9, 123.9, 121.3; m/z (ASAP-MS, ESI+) calcd for $C_{22}H_8O_6S_2$ $[M]^+$ 431.9768; found 431.9776.

**Tri-*n*-butyl(naphthalen-2-yl)stannane**[13]

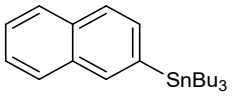


To a commercially available solution of (naphthalen-2-yl)-magnesium bromide (0.5 M in THF, 30 ml 15 mmol) in THF (30 ml) under an Ar atmosphere at 0 °C, was added tri-*n*-butyltin chloride (4.88 g, 15 mmol) dropwise. The resulting dark brown suspension was allowed to return to room temperature and stirred overnight. To this was added $NaOH_{(aq)}$ (1 M, 15 mL) and stirred for 1 h, then diluted with EtOAc (100 ml), separated, washed with brine (2 x 15 mL), dried with $MgSO_4$ and concentrated to dryness. The resulting clear oil was purified by Kugelrohr distillation (200 °C, 0.3 Torr) to give the title product (4.59 g, 73%) as a semi-crystalline oil, identical by NMR with the literature.[14] $^1$H NMR (500 MHz, $CDCl_3$) δ 8.01-7.92 (m, 1H), 7.86-7.78 (m, 3H), 7.63-7.54 (m, 1H), 7.51-7.45 (m, 2H), 1.61 (tt, *J* = 8.2, 6.3 Hz, 6H), 1.42-1.35 (*app* h, *J* = 7.3 Hz, 6H), 1.22-1.09 (m, 6H) 0.92 (t, *J* = 7.3 Hz, 9H); $^{13}$C NMR (125 MHz, $CDCl_3$): δ 139.8, 136.7, 133.5, 133.4, 133.0, 127.9, 127.7, 126.9, 125.8, 125.8, 29.3, 27.5, 13.8, 9.8.

***4,9-di(anthracen-9-yl)isochromeno[6,5,4-def]isochromene-1,3,6,8-tetraone* 1e**

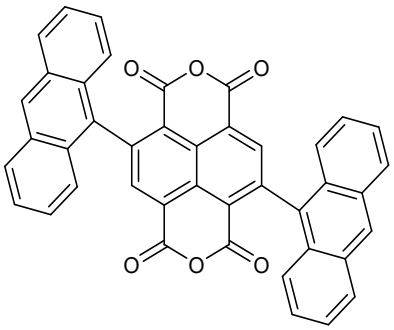


**1e**

2,6-Dibromo-1,4,5,8-naphthalenetetracarboxylic dianhydride **$Br_2$NDA** (0.75 g, 1.76 mmol, 1.0 eq) and anthracen-9-yltributylstannane (prepared following a literature procedure[14]) (2.468 g, 5.282 mmol, 3.0 eq) in PhCl (12 mL) in the presence of $PdCl_2(PPh_3)_2$ (123 mg, 0.177 mmol, 0.1 eq) were reacted according to **General Method 1** to give the desired product **1e** as a dark purple solid (0.583 g, 53%). $^1$H NMR (500 MHz, DMSO) δ 8.84 (s, 2H), 8.44 (s, 2H), 8.27 (d, *J* = 8.6 Hz, 4H), 7.60 (t, *J* = 7.3 Hz, 4H), 7.51 (app. d, *J* = 8.6 Hz, 4H), 7.44 (app. t, *J* = 6.6 Hz, 4H); $^{13}$C NMR (126 MHz, DMSO) δ 159.5, 157.3, 144.2, 135.9, 133.4, 131.0, 129.8, 128.8, 128.7, 127.6, 126.3, 125.5, 125.4, 125.1, 124.1; IR $\nu_{max}$ ($cm^{-1}$) 3048, 1790, 1737, 1575, 1422; m/z (ASAP-MS, ESI+) calcd for $C_{42}H_{20}O_6$ $[M+H^+]$: 621.1333; found: 621.1329.

***3,3'-(1,3,6,8-Tetraoxo-4,9-diphenyl-1,3,6,8-tetrahydrobenzo[lmn][3,8]phenanthroline-2,7-diyl)dipropionic acid*** **NDI-Ph**

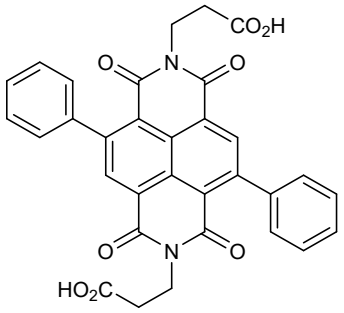

**NDI-Ph**

4,9-Diphenylisochromeno[6,5,4-def]isochromene-1,3,6,8-tetraone **1a** (0.200 g, 0.48 mmol), was mixed with β-alanine (0.127 g, 1.43 mmol, 3.0 eq) in glacial AcOH (2 mL) and reacted according to **General Method 2** to give the product as a yellow solid (0.183 g, 68%).

$^{1}$H NMR (500 MHz, DMSO) δ 12.28 (s, 2H), 8.36 (s, 2H), 7.54 – 7.46 (m, 10H), 4.15 (t, *J* = 7.6 Hz, 4H), 2.54 (t, *J* = 7.6 Hz, 4H); $^{13}$C NMR (126 MHz, DMSO) δ 172.3, 162.1, 161.9, 146.1, 140.7, 134.4, 128.3, 128.2, 127.9, 126.8, 125.5, 123.0, 36.2, 31.9; m/z (ASAP-MS, ESI+) calcd for $C_{32}H_{21}N_2O_8$ $[M-H]^+$ 561.1303; found 561.1289.

***3,3'-(4,9-dimesityl-1,3,6,8-tetraoxo-1,3,6,8-tetrahydrobenzo[lmn][3,8]phenanthroline-2,7-diyl)dipropionic acid*** **NDI-Mes**

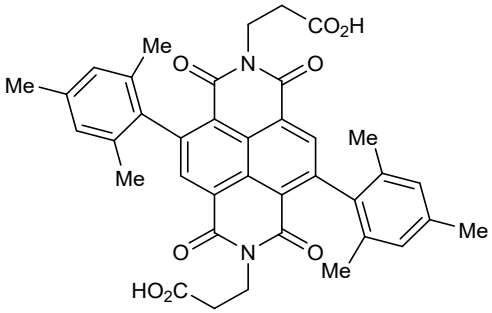

**NDI-Mes**

This product was produced by adaptation of **General Method 2**. Thus, 4,9-dimesityl-isochromeno[6,5,4-def]isochromene-1,3,6,8-tetraone **1b** (0.400 g, 0.793 mmol), was mixed with β-alanine (0.283 g, 3.171 mmol, 4.0 eq) in DMF (5 mL) and reacted to give the crude product. This was filtered and washed with EtOAc (3 x 5 mL), giving **NDI-Mes** as a dark yellow solid (0.216 g, 85%). $^{1}$H NMR (500 MHz, DMSO) δ 12.32 (s, 2H), 8.16 (s, 2H), 6.99 (s, 4H), 4.12 (t, *J* = 7.7 Hz, 4H), 2.52 (t, *J* = 7.7 Hz, 4H), 2.34 (s, 6H), 1.86 (s, 12H); $^{13}$C NMR (126 MHz, DMSO) δ 172.3, 162.2, 161.5, 145.2, 137.6, 136.1, 133.7, 133.4, 128.1, 126.9, 126.5, 123.8, 36.0, 31.9, 20.8, 20.2; IR $\nu_{max}$ ($cm^{-1}$) 2971, 2918, 1721, 1706, 1670, 1576, 1438; m/z (ASAP-MS, ESI+) calcd for $C_{38}H_{34}N_2O_8$ $[M+H]^+$ 647.2388; found 647.2388.

***3,3'-(1,3,6,8-Tetraoxo-4,9-di(thiophen-2-yl)-1,3,6,8-tetrahydrobenzo[lmn][3,8]phenanthroline-2,7-diyl)dipropionic acid*** **NDI-Th**

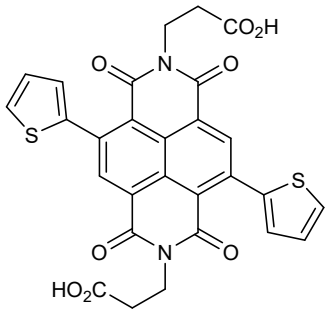


**NDI-Th**

4,9-Di(thiophen-2-yl)isochromeno[6,5,4-def]isochromene-1,3,6,8-tetraone **1c** (0.200 g, 0.463 mmol), was mixed with β-alanine (0.124 g, 1.388 mmol, 3.0 eq) in glacial AcOH (2 mL) and reacted according to **General Method 2** to give the product as a bright red solid (0.174 g 66%). $^{1}$H NMR (500 MHz, DMSO) δ 12.34 (s, 2H), 8.46 (s, 2H), 7.82 (dd, *J* = 5.1, 1.2 Hz, 2H), 7.44 (dd, *J* = 3.6, 1.2 Hz, 2H), 7.22 (dd, *J* = 5.1, 3.6 Hz, 2H), 4.19 (t, *J* = 7.7 Hz, 4H), 2.57 (t, *J* = 7.7 Hz, 4H); $^{13}$C NMR (126 MHz, DMSO) δ 172.3, 161.8, 161.7, 140.4, 138.6, 135.0, 129.0, 128.6, 127.6, 127.1, 125.5, 123.3, 36.3, 31.9; m/z (ASAP-MS, ESI+) calcd for $C_{28}H_{18}N_2O_8S_2$ $[M-H]^+$ 573.0432; found 573.0421.

***3,3'-(4,9-Di(naphthalen-2-yl)-1,3,6,8-tetraoxo-1,3,6,8-tetrahydrobenzo[lmn][3,8]-phenanthroline-2,7-diyl)dipropionic acid*** **NDI-Nap**

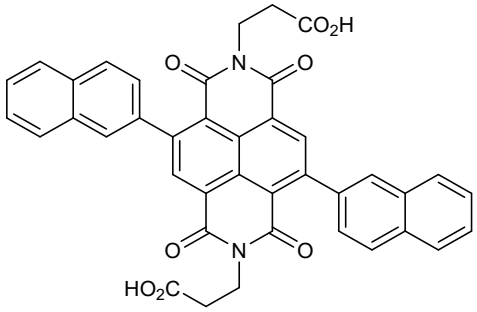


**NDI-Nap**

2,6-Dibromo-1,4,5,8-naphthalenetetracarboxylic dianhydride **$Br_2$NDA** (0.50 g, 1.174 mmol, 1.0 eq) and tri-*n*-butyl(naphthalen-2-yl)stannane (1.22 g, 2.917 mmol, 2.5 eq) in PhCl (8 mL) in the presence of $PdCl_2(PPh_3)_2$ (82 mg, 0.117 mmol, 0.1 eq) were reacted according to **General Method 1** to give 4,9-di(naphthalen-2-yl)isochromeno[6,5,4-def]isochromene-1,3,6,8-tetraone **1d** as a brown solid (0.580 g, 95%).

This was used without purification in the next step by adaptation of **General Method 2**. Thus, **1d** (0.200 g, 0.384 mmol), was mixed with β-alanine (0.103 g, 1.15 mmol, 3.0 eq) in DMF (2 mL) and reacted to give the crude product. This was filtered and washed with EtOAc (3 x 5 mL) giving **NDI-Nap** as a sandy yellow solid (0.216 g, 85%). $^{1}$H NMR (500 MHz, DMSO) δ 8.55 (s, 2H), 8.07 – 7.97 (m, 8H), 7.66 – 7.56 (m, 6H), 4.20 (t, *J* = 7.4 Hz, 4H), 2.55 (t, *J* = 7.4 Hz, 4H) m/z (ASAP-MS, ESI+) calcd for $C_{40}H_{26}N_2O_8$ $[M-H]^+$ 661.1605; found 661.1608.

***3,3'-(4,9-di(anthracen-9-yl)-1,3,6,8-tetraoxo-1,3,6,8-tetrahydrobenzo[lmn][3,8]phenanthroline-2,7-diyl)dipropionic acid*** **NDI-An**

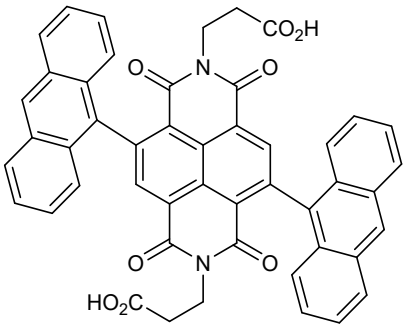


**NDI-An**

This product was produced by adaptation of **General Method 2**. Thus, 4,9-di(anthracen-9-yl)isochromeno[6,5,4-def]isochromene-1,3,6,8-tetraone **1e** (0.250 g, 0.40 mmol), was mixed with β-alanine (0.144 g, 1.61 mmol, 4.0 eq) in DMF (2 mL) and reacted to give the crude product which was diluted with water (10 mL) filtered and washed with water (10 mL), $Et_2O$ (10 mL) then EtOH (10 mL) and dried giving **NDI-An** as a dark purple solid (0.271 g, 88%). $^1$H NMR (500 MHz, DMSO) δ 12.23 (s, 2H), 8.80 (s, 2H), 8.37 (s, 2H), 8.25 (d, *J* = 8.6 Hz, 4H),7.58 (t, *J* = 7.4 Hz, 4H), 7.50 (d, J = 8.7 Hz, 1H), 7.41 (t, *J* = 7.4 Hz, 4H), 3.95 (t, *J* = 7.8 Hz, 4H), 2.33 (t, *J* = 7.8 Hz, 4H); $^{13}$C NMR (126 MHz, DMSO) δ 172.4, 162.8, 162.1, 143.8, 136.0, 135.6, 131.9, 129.3, 129.1, 128.5, 127.3, 127.3, 126.7, 126.3, 125.9, 125.7, 36.5, 34.3, 32.0; IR $\nu_{max}$ ($cm^{-1}$) 1704, 1663, 1578, 1442; m/z (ASAP-MS, ESI+) calcd for $C_{48}H_{30}N_2O_8$ $[M+H]^+$ 763.2075; found 763.2073.

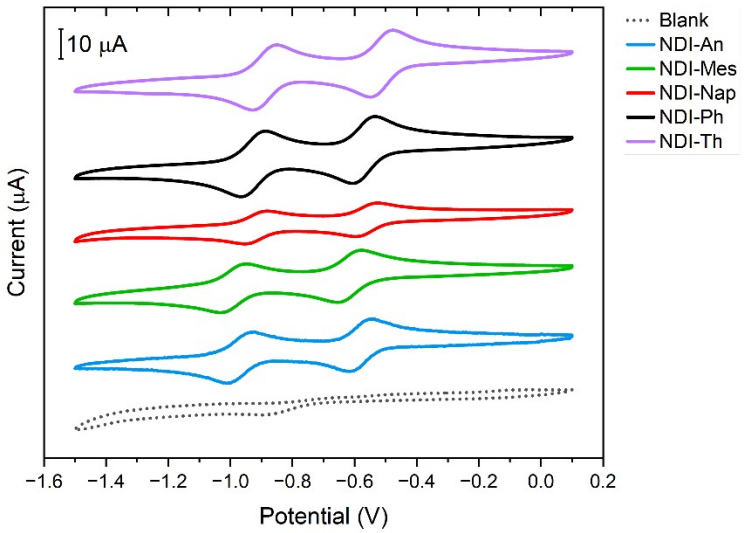


**Figure S1.** Cyclic voltammetry of the molecules studied: **NDI-Ph** (black), **NDI-Nap** (red), **NDI-An** (blue), **NDI-Mes** (green) and **NDI-Th** (purple) with a $Ag/AgNO_3$ reference electrode in a DMF $TBAPF_6$ solution. A blank CV has been added to the graph.

## 3. Electrochemical Analysis

| Molecule | $E^0_{red1}$ (V)[a] | $E^0_{red2}$ (V)[a] | $E_{onset}$ (V)[b] | EA (eV)[c] |
|---|---|---|---|---|
| **NDI-Th** | -0.55 | -0.93 | -0.44 | 3.9 |
| **NDI-Ph** | -0.61 | -0.97 | -0.50 | 3.8 |
| **NDI-Nap** | -0.60 | -0.95 | -0.49 | 3.8 |
| **NDI-Mes** | -0.65 | -1.03 | -0.54 | 3.8 |
| **NDI-An** | -0.62 | -1.01 | -0.52 | 3.8 |

[a] $E^0_{red1/2}$ – potential of the first or second reduction peak respectively

[b] $E_{onset}$ – first reduction potential onset

[c] EA – electron affinity, $EA = E_{onset} - E_{onset\ Fc/Fc+\ vs\ Ag/AgCl} - 4.8$

**Table S1.** Parameters obtained from the cyclic voltammery of the studied compounds.

# 4. Spectroscopic Analysis

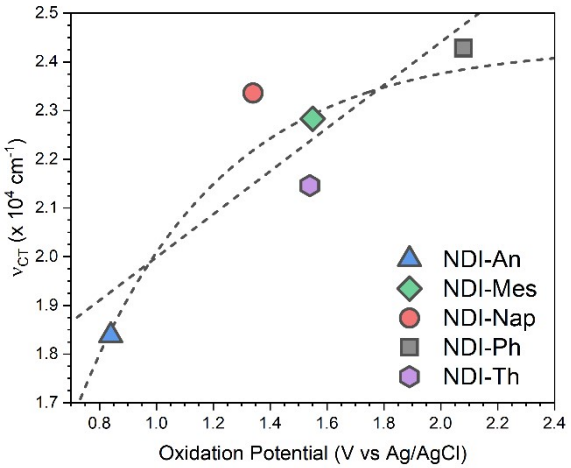


**Figure S2.** Mulliken dependence of the charge-transfer energy in the series of NDI molecules studied. Linear and asymptotic fits have been added to help the eye. The oxidation potential has been taken from main text references 63-65.

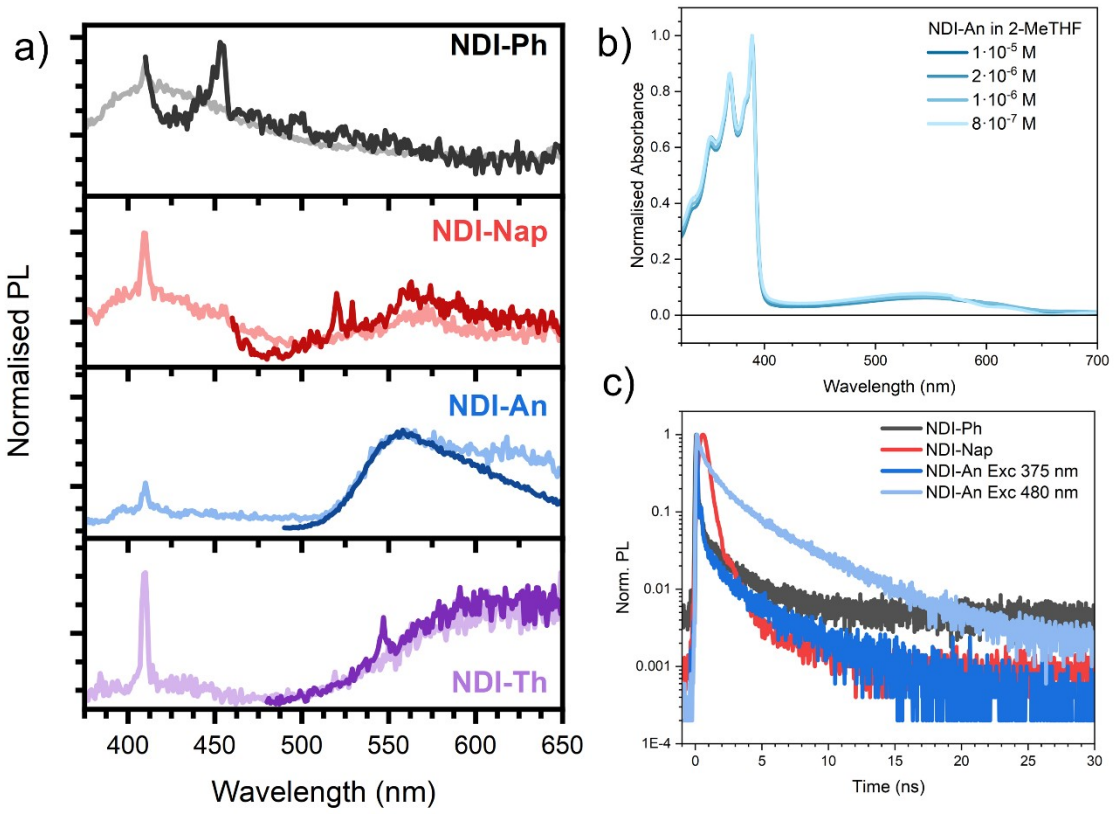


d)

| Compound | Absorptivity (x $10^3$ $M^{-1}$ $cm^{-1}$) |
|---|---|
| NDI-Ph | 7.78 |
| NDI-Nap | 8.74 |
| NDI-An | 67.4 |
| NDI-Th | 1.83 |

**Figure S3.** a) Fluorescene spectra of 2-MeTHF solutions of **NDI-Ph** (black), **NDI-Nap** (red), **NDI-An** (blue) and **NDI-Th** (purple), exciting the NDI moiety at 365 nm (lighter trace) for all derivatives, and the CT band (darker trace) at 400, 450, 480 and 470 nm for **NDI-Ph**, **NDI-Nap**, **NDI-An** and **NDI-Th**, respectively. Notice the sharp 409 nm signal of 2-MeTHF Raman when exciting at 365 nm. b) NDI-An absorbance in a wide range of concentrations that go from $10^{-5}$ to $8{\cdot}10^{-7}$ M. For the highest concentrations we used a 1 mm cuvette to avoid spectrophotometer saturation. c) Fluorescence decays of 2-MeTHF solutions of **NDI-Ph** (black), exciting at 405 nm, **NDI-Nap** (red) , exciting at 375 nm, and **NDI-An** (blue), exciting at 375 and 480 nm (darker and lighter blue, respectively). Decays were probed at 560 nm. d) Absorptivity for the studied compounds in 2-MeTHF with concentrations in the range of $10^{-5}$ M with a 1 cm cuvette.

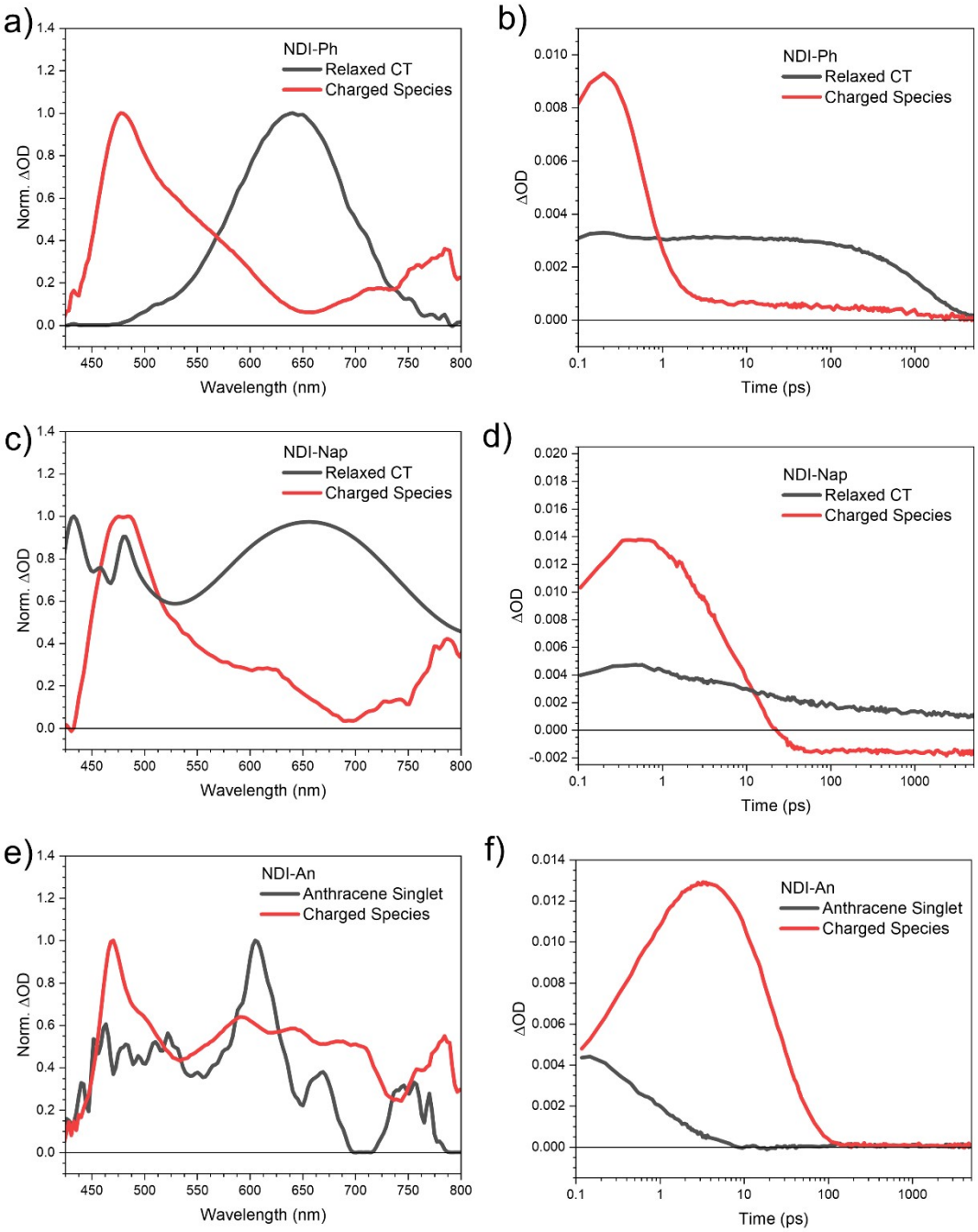


**Figure S4.** Results of the Global Analysis mathematical treatment for **NDI-Ph** (a,b), **NDI-Nap** (c,d) and **NDI-An** (e,f). Spectra of the associated species are shown in a, c and e while decays are shown in b, d and f.

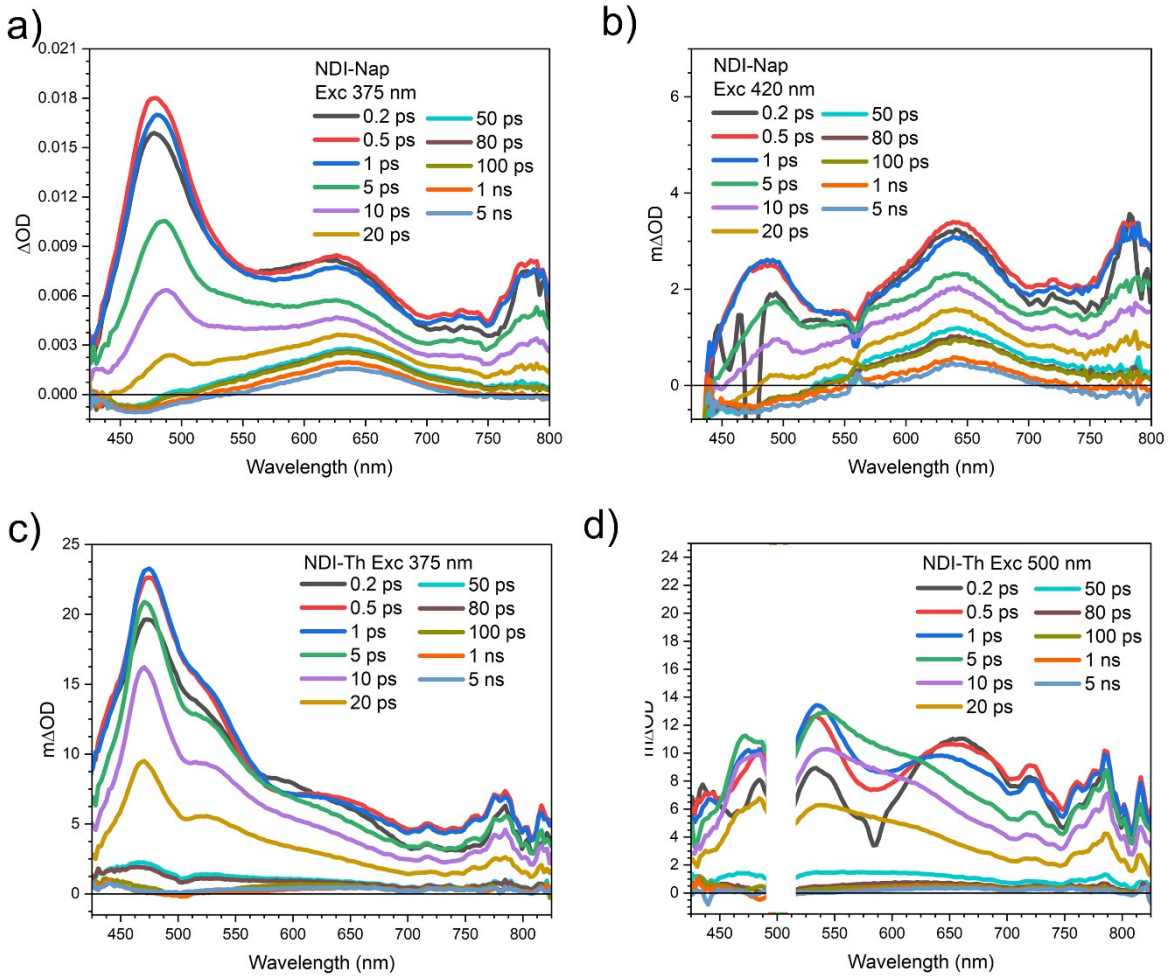


**Figure S5.** Femtosecond transient absorption data of 2-MeTHF solutions of **NDI-Nap** upon excitation at a) 375 and b) 420 nm and **NDI-Th** upon excitation at c) 375 and d) 500 nm. Excitation density was maintained at 0.25 mW.

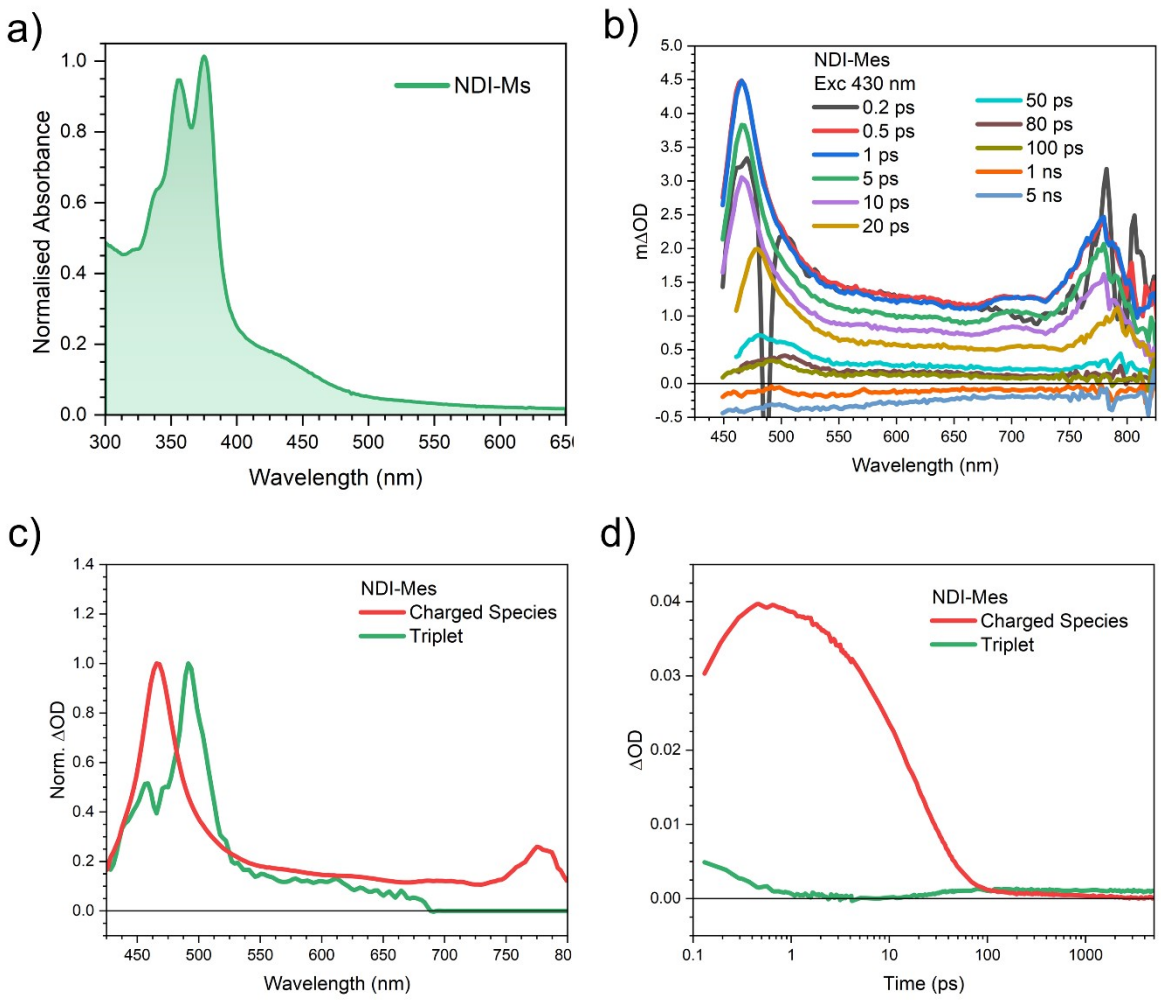


**Figure S6.** Results of the **NDI-Mes** characterisation: a) Ground state absorbance with an absorptivity at 375 nm of 2.2 $10^4$ $M^{-1}$ $cm^{-1}$, b) femtosecond transient absorption data of 2-MeTHF solutions upon excitation at 430 nm, and (c,d) the global analysis mathematical treatment for **NDI-Mes.** Excitation density was maintained at 0.25 mW.

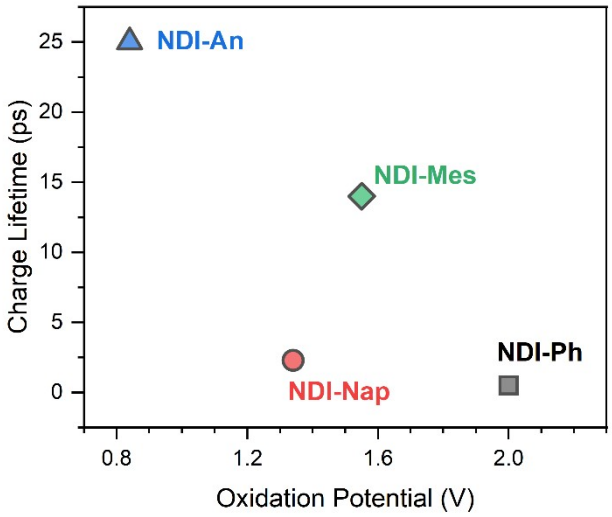


**Figure S7.** Relationship between the charge lifetime and the oxidation potential of the core substituent: **NDI-Ph** (black square), **NDI-Nap** (red circle), **NDI-An** (blue triangle) and **NDI-Mes** (green diamond). Oxidation potentials vs Ag/AgCl have been taken from main text references 63 and 65. The oxidation potential represents a good approximation to donor strength since the NDI core, the acceptor, is the same for all of them.

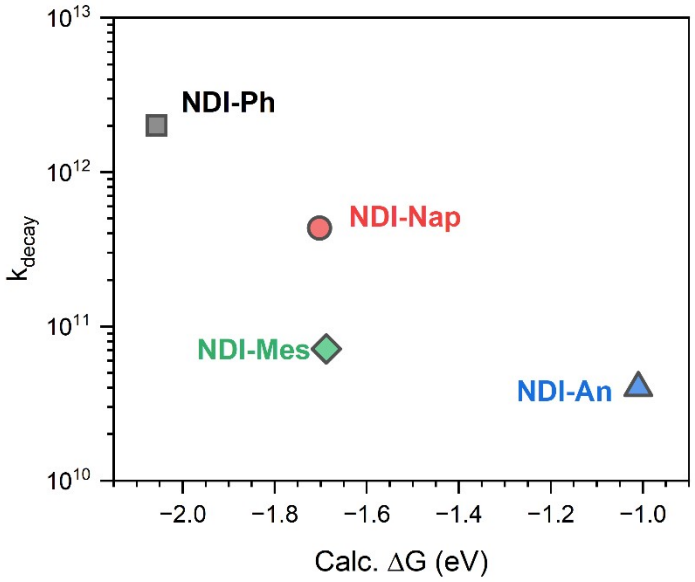


**Figure S8.** Marcus theory relationship between the charge decay rate and the calculated difference of the gibbs energy between the charged excited and ground states for **NDI-Ph** (black square), **NDI-Nap** (red circle), **NDI-An** (blue triangle) and **NDI-Mes** (green diamond). Calculations have been done for reduced models to optimise the computing resources (more details in the Calculations section). Notice that since the rates are for the decays from the charged state to the ground state, the ΔG are also calculated from the charged excited to ground states.

# 5. Theoretical Calculations

## Theoretical calculation methods

First, we performed a benchmark of different DFT functionals and basis sets to try and reproduce the absorption spectra. The method which provided best results was TD-B3LYP-D3/def2-SVP. The five NDIs were optimised (see the structures in Figure S1) and its Raman and IR spectra were calculated until no imaginary frequencies were found.

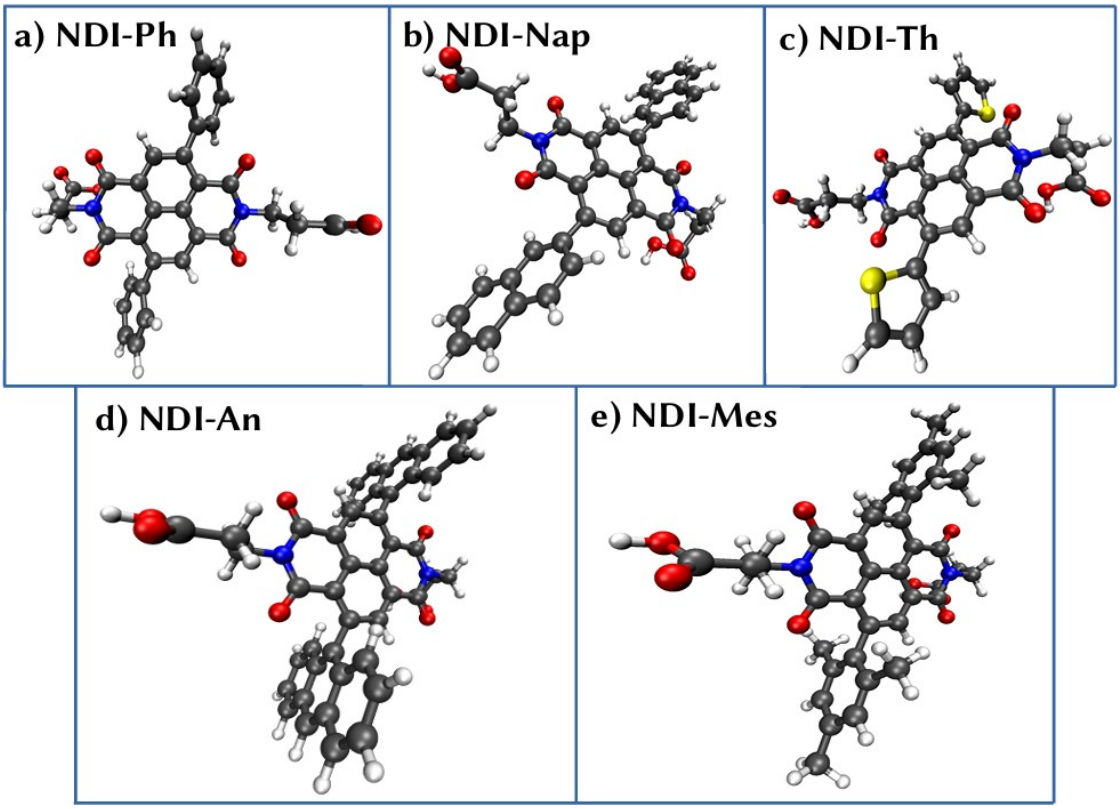


**Figure S9.** Optimized molecular structures of the four cases of study: **(a) NDI-Ph**, **(b) NDI-Nap**, **(c) NDI-Th**, **(d) NDI-An**, and **(e) NDI-Mes**. The optimization was performed using TD-B3LYP-D3/def2-SVP level of theory.

A relaxed potential energy scan was performed by modifying the torsional angle between the NDI core and one of the substituents. For the case of **NDI-Ph**, we observed a relative stabilization of the energy at 60º and 120º torsional angle in comparison to the fully perpendicular orientation at 90º. This is due to a hydrogen bond formation between one of the phenyl hydrogens and the oxygen in the NDI core of the molecule. Figure S8 includes the optimized structures along the torsional angle showing the O-H distance of the mentioned hydrogen bond.

The energy barriers of these scans have been included in both panels of Figure S9 and in Figure 4a in the manuscript. By looking at the right panel, we can see that the **NDI-Th** shows a much lower barrier in comparison with the other compounds, due to the absence of the H atom colliding with the O of the NDI core, favoring the rotation of the thiophene.

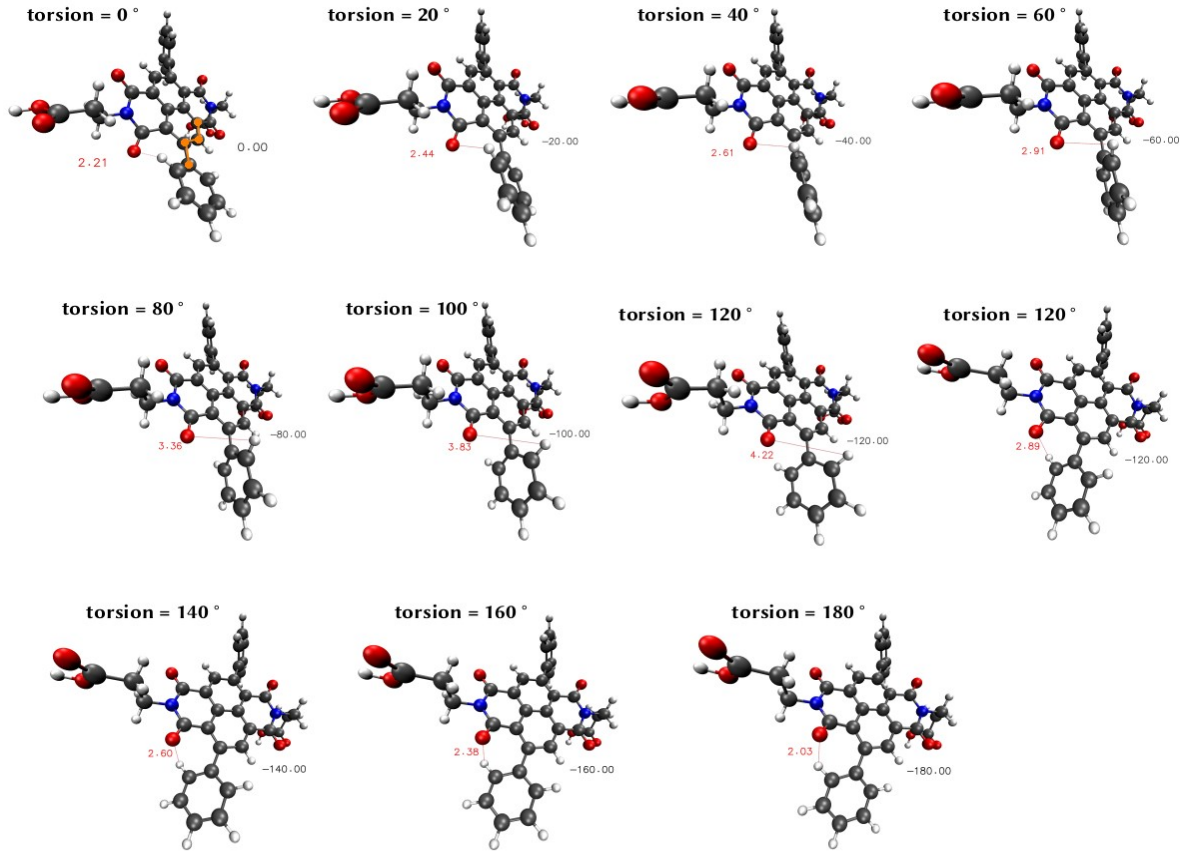


**Figure S10.** Hydrogen bonds for **NDI-Ph** formed upon rotation of the dihedral marked in orange.

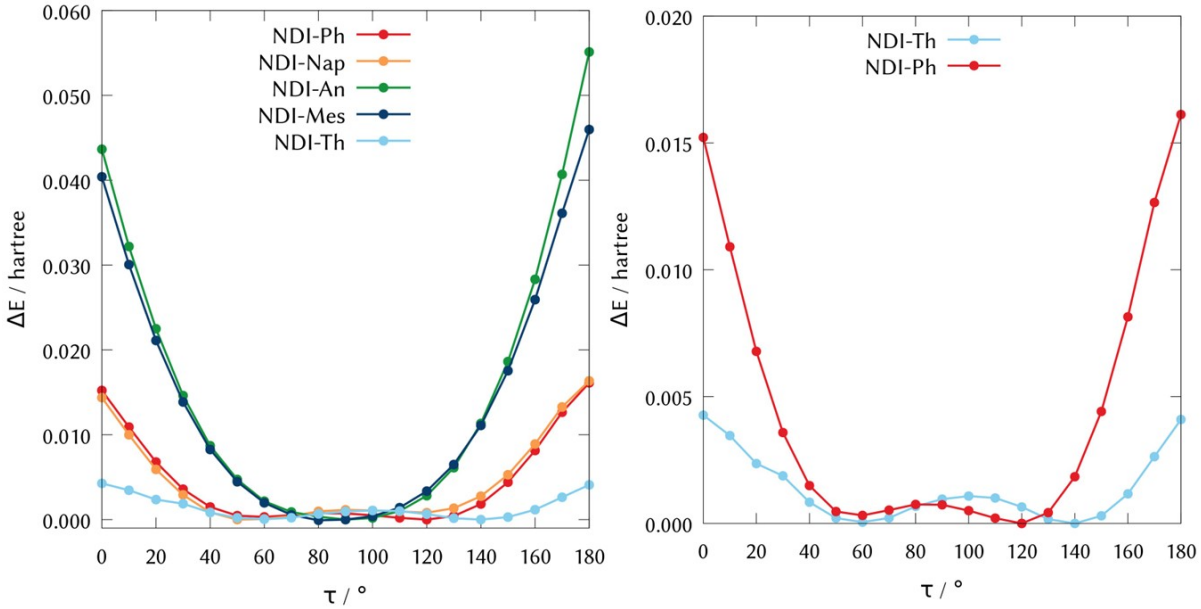


**Figure S11.** Relaxed potential energy scans along the torsional angle between the NDI core and the substituents.

The nuclear ensemble method has been used to compute the vertical absorption spectra of the four molecules. TD-B3LYP-D3/def2-SVP vertical energies from 10 initial conditions of a Wigner distribution to emulate the vibrational ground state were calculated to obtain the vibrational corrected absorption spectra represented in **Figure S12**.

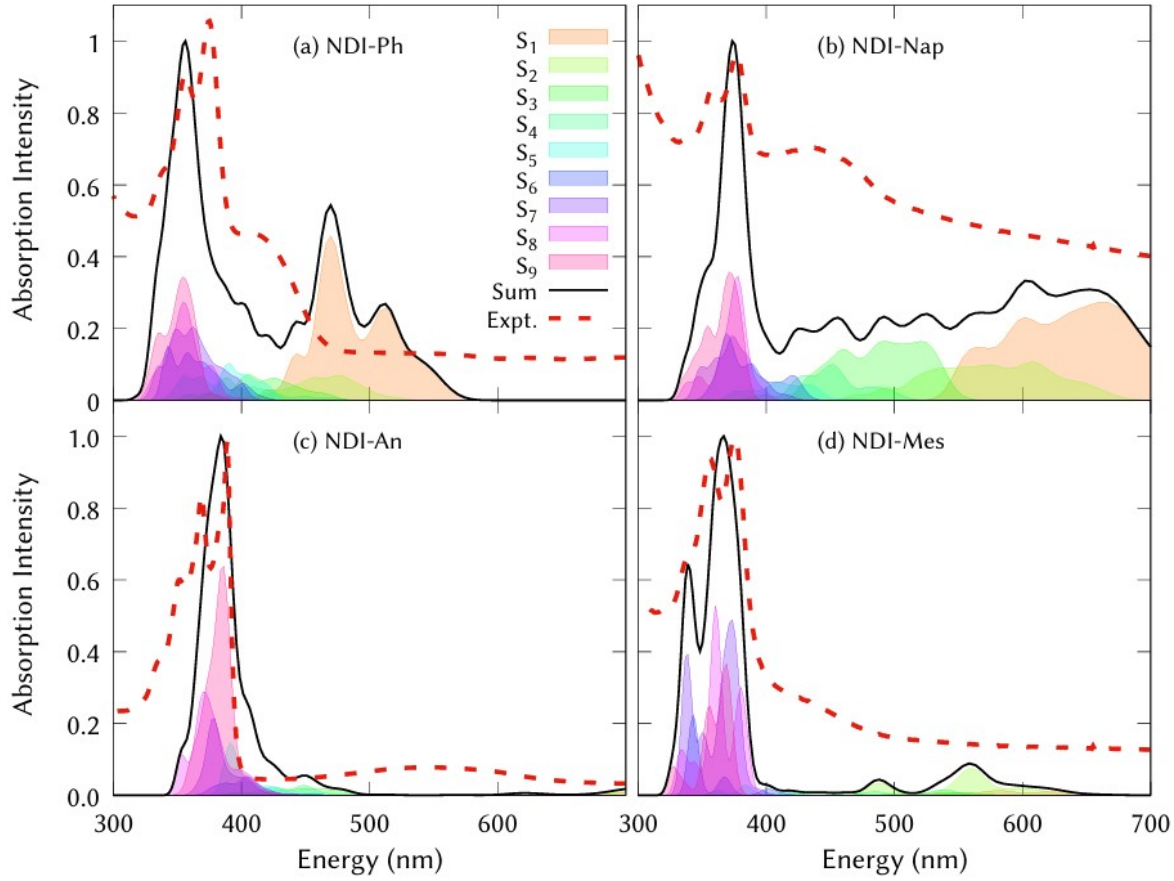


**Figure S12.** Vertical absorption spectra of (a) **NDI-Ph**, (b) **NDI-Nap**, (c) **NDI-An**, (d) **NDI-Mes** calculated using TD-B3LYP-D3/def2-SVP method and exciting 50 initial conditions from a Wigner distribution. The calculated spectra was shifted 0.15 eV for the **NDI-An** case. Experimental spectra for the four cases are included in dashed red lines.

## Electronic Coupling calculations

To quantify the electronic coupling associated with charge-transfer processes we employed the generalized Mulliken-Hush (GMH) and fragment charge difference (FCD) schemes as implemented in Q-Chem. To perform these calculations we used NDI-H truncated models, with a single donor unit, the substituent, and the NDI core, to economise calculations. These calculations were performed at the TD-DFT level using the first excited state identified as a charge transfer state. Within the two-state approximation, the diabatic donor and acceptor states are constructed as linear combinations of eigenstates, determined by zero transition dipoles in the GMH scheme or by maximum charge differences in the FCD scheme for the donor and acceptor fragments. The donor and acceptor fragments were explicitly defined, and the couplings were evaluated to represent the interaction between the ground state and the selected charge transfer excited state. The electron transfer rate $k_{ET}$ has been computed using the FCD coupling value at 273 K, after optimising the $S_1$ electronic state minima structures.

**GMH**:

$$V_{ET} = (E_n - E_m)\frac{\|\mu_{mn}\|}{\sqrt{(\mu_m - \mu_n)^2 + 4\|\mu_{mn}\|^2}}$$

**FCD**:

$$V_{ET} = (E_n - E_m)\frac{\Delta\bar{q}_{mn}}{\sqrt{(\Delta q_m - \Delta q_n)^2 + 4(\Delta\bar{q}_{mn})^2}}$$

**Table S2.** Comparison of donor-acceptor electronic couplings in our molecules using fragment charge difference (FCD) and generalised Mulliken Hush (GMH) analyses.

| Molecule | $H_{DA}^{FCD}$ (eV) [(a)] | $H_{DA}^{GMH}$ (eV) [(b)] |
|---|---|---|
| NDI-Ph | 0.353 | 0.326 |
| NDI-Nap | 0.162 | 0.174 |
| NDI-Mes | 0.055 | 0.057 |
| NDI-An | 0.031 | 0.032 |

[(a)] The electronic couplings computed using the fragment charge difference (FCD).
[(b)] The electronic couplings computed using the generalized Mulliken-Hush (GMH) scheme.

## Excited state characterisation:

We also characterised the excited states, finding that in the anthracene compound, the charge transfer (CT) band was shifted to lower wavelengths and is the equivalent to the main locally excited (LE) band in the benzene compound. The molecular orbitals (MOs) for the benzene and anthracene compounds are schematized in Figure S11.

A detailed description of the MOs involved in the peaks of the absorption spectra of the phenyl (**NDI-Ph**) and anthracene (**NDI-An**) are collected in Figures S12 and S13, respectively.

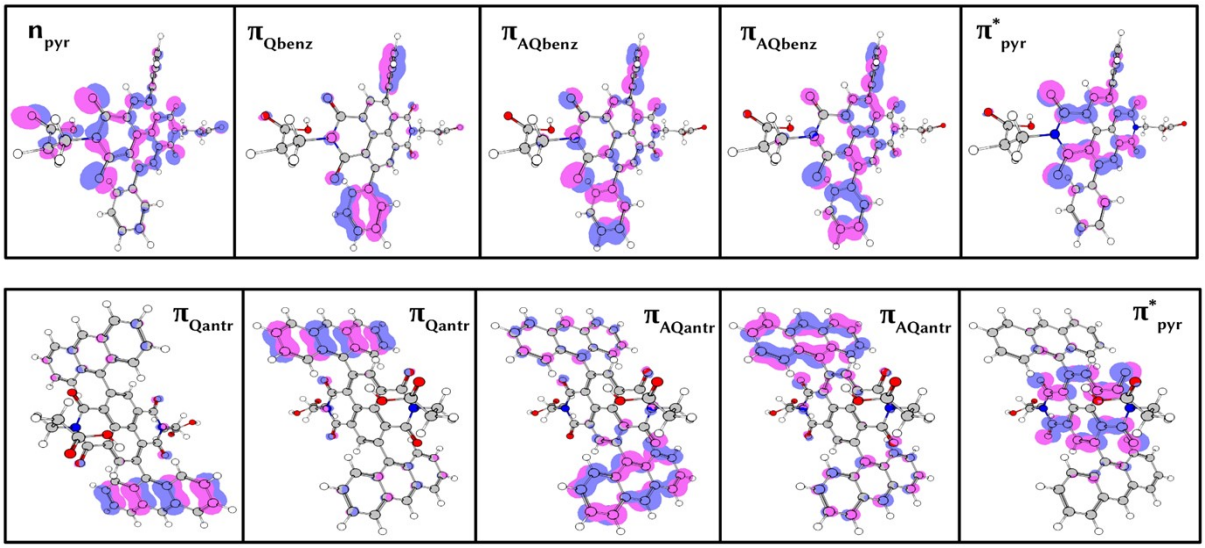


**Figure S14.** Molecular orbitals involved in the lowest excited states of **NDI-Ph** (upper panels) and **NDI-An** (lower panels) calculated using TD-B3LYP-D3/def2-SVP method.

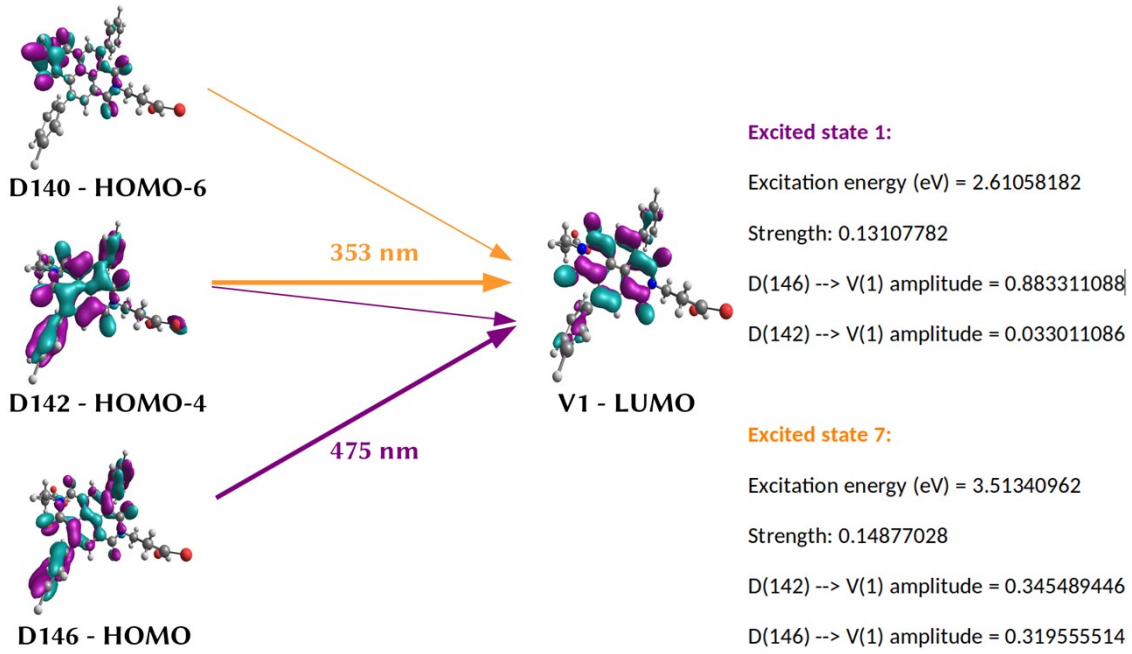


**Figure S15.** Molecular orbitals involved in the main (brightest) transitions of **NDI-Ph** calculated using TD-B3LYP-D3/def2-SVP method.

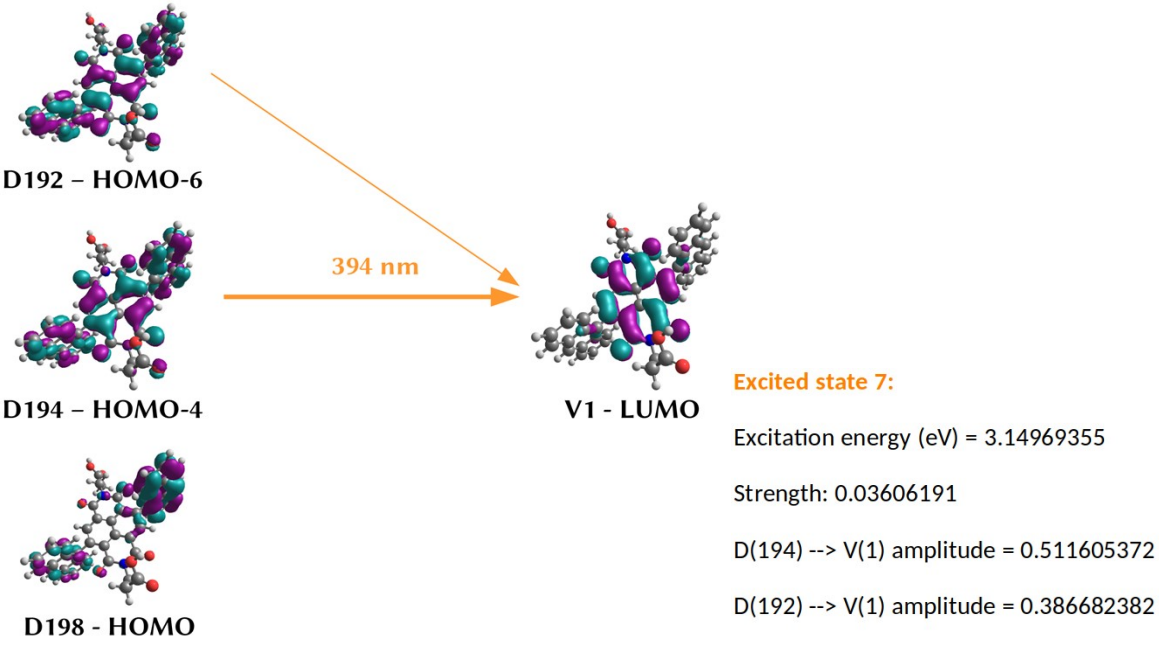


**Figure S16.** Molecular orbitals involved in the main transitions of **NDI-An** calculated using TD-B3LYP-D3/def2-SVP method. Extract from output specifying contributions to the brightest excited state (state 7).

## Nonadiabatic dynamics calculations from the electronic excited states:

To run dynamics simulations we chose the **NDI-Ph** and **NDI-An** compounds, since they show the most distinct behaviour. We decided to fit linear vibronic coupling model coupled surfaces to run ML-MCTDH quantum dynamics. The number of coupled states has been selected based on the density of states of each system, i.e., number of states within an energy range, represented in Figure S14 for these two systems.

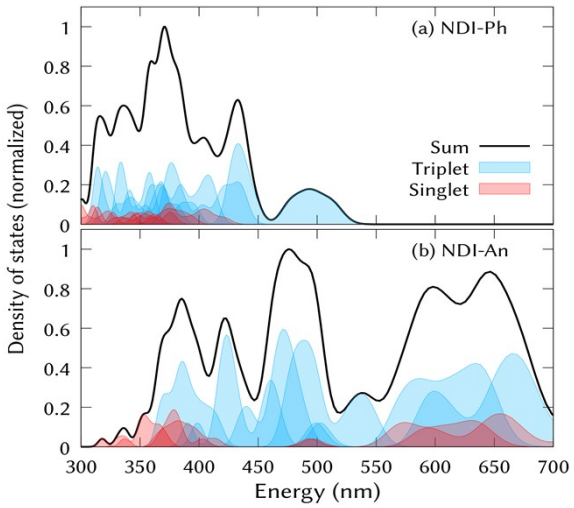


**Figure S17.** Density of singlet (red) and triplet (blue) excited states in the relevant energy range for **NDI-Ph** and **NDI-An** calculated using TD-B3LYP-D3/def2-SVP method and exciting 50 initial conditions from a Wigner distribution.

Based on the calculated density of states, we parametrised the model potentials. For **NDI-Ph** the model had five electronic singlet states, four electronic triplet states along the 186 vibrational modes and for **NDI-An** the model had five singlet states, two triplet states and 258 vibrational modes.

We ran fully converged ML-MCTDH nonadiabatic dynamics on the model potentials for 1.2 picoseconds and found that the deactivation in **NDI-Ph** is several orders of magnitude faster than in **NDI-An**, i.e., the local excited states (LE) are shorter lived than the charge transfer (CT) ones, as we can see in the transient absorption spectra.

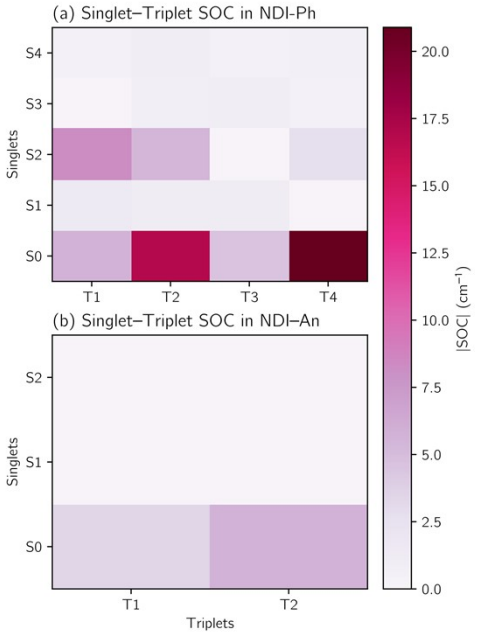


**Figure S18.** Spin-orbit copling (SOC) matrix elements at the ground state optimised geometry calculated with the TD-B3LYP-D3/def2-SVP level of theory for a) **NDI-Ph** and b) **NDI-An**. This matrix enters in the molecular electronic Hamiltonian as $H_{SOC}$, coupling the relevant electronic states during the nonadiabatic molecular dynamics.

## Marcus Theory Calculations

The Gibbs free energies of the ground and first excited states have been simulated for reduced models, for computing optimisation, of the four studied compounds (i.e., with only one substituent **NDI-PhH**, **NDI-NapH**, **NDI-MesH** and **NDI-AnH**). The rate constants used for the graph are the decay rates for the charged states, since the electron transfer rates are faster than the detection limit of the fs-TAS technique. However, the electron transfer from the substituent to the NDI core to form the charged species is equivalent to the electron transfer from the NDI core to the positive charged substituent.[15]

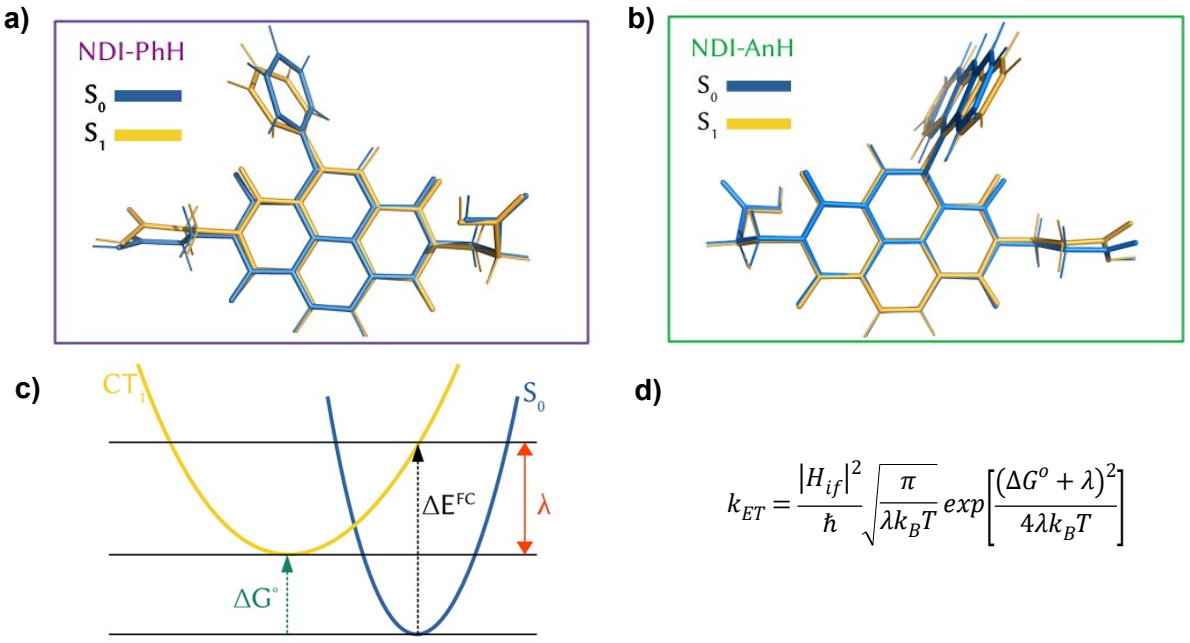


**Figure S19.** Geommetry optimisation of ground state and the first excited state of **a)** NDI-PhH and **b)** NDI-AnH. NDI-XH is the truncated asymmetric derivative with only one substituent to optimise the computation time. **c)** Scheme depicting the energetic values calculated for the studied molecules. Equation used for the calculations of the kinetic rates.

**Table S3.** Calculated energetics for the studied molecules.

| Molecule | $\Delta E^{FC}$ (eV) | $\Delta E^{S_1}$ (eV) | $\lambda$ (eV) | $\Delta G^o$ (eV) | $k_{ET}$ [(a)] ($s^{-1}$) |
|---|---|---|---|---|---|
| NDI-Ph | 2.610 | 1.005 | 4.667 | -2.057 | $1.688 \cdot 10^7$ |
| NDI-Nap | 1.908 | 1.252 | 3.611 | -1.703 | $3.274 \cdot 10^8$ |
| NDI-Mes | 2.170 | 1.058 | 3.858 | -1.688 | $4.621 \cdot 10^6$ |
| NDI-An | 1.342 | 0.715 | 2.352 | -1.010 | $1.572 \cdot 10^8$ |

[(a)] The k electron-transfer (ET) rate constant has been computed using the FCD coupling value at 293.15 K.

# 6. Crystallographic data

**Table S4.** Crystallographic information and details of refinement parameters of the **NDI-Th**, **NDI-Ph** and **NDI-An** structures.

| | **NDI-Th THF solvate** | **NDI-Ph THF solvate** | **NDI-An diethyl ether solvate** | **NDI-An diethyl-ether THF solvate** |
|---|---|---|---|---|
| empirical formula | $C_{36}H_{34}N_2O_{10}S_2$ | $C_{40}H_{38}N_2O_{10}$ | $C_{56}H_{50}N_2O_{10}$ | $C_{53.33}H_{41.33}N_2O_{9.33}$ |
| $M_r$ / g mol$^{-1}$ | 512.52 | 706.72 | 910.98 | 859.45 |
| crystal system | monoclinic | monoclinic | triclinic | triclinic |
| space group | $P2_1/n$ | $P2_1/n$ | $P\bar{1}$ | $P\bar{1}$ |
| $a$ / Å | 12.9774(2) | 12.65610(10) | 9.5740(4) | 12.3074(2) |
| $b$ / Å | 5.86680(10) | 6.01420(10) | 10.9624(4) | 12.7452(2) |
| $c$ / Å | 21.8939(3) | 22.4821(2) | 12.4555(5) | 21.9715(4) |
| $\alpha$ / ° | 90 | 90 | 65.247(4) | 73.849(2) |
| $\beta$ / ° | 91.1850(10) | 92.0920(10) | 75.551(3) | 77.125(2) |
| $\gamma$ / ° | 90 | 90 | 89.276(3) | 76.785(2) |
| $V$ / Å$^3$ | 1666.55(4) | 1710.11(3) | 1143.29(8) | 3175.70(10) |
| $Z$ | 2 | 2 | 1 | 3 |
| $\rho_{calc}$ / g cm$^{-3}$ | 1.432 | 1.372 | 1.323 | 1.348 |
| $T$ / K | 150.0(1) | 150.0(1) | 100.0(1) | 150.0(1) |
| $\mu$ / mm$^{-1}$ | 1.982 | 0.820 | 0.739 | 0.757 |
| $F$(000) | 752.0 | 744.0 | 480.0 | 1350 |
| crystal size / mm$^3$ | 0.33 × 0.06 × 0.04 | 0.35 × 0.04 × 0.04 | 0.28 × 0.13 × 0.07 | 0.09 × 0.06 × 0.03 |
| radiation | Cu $K\alpha$ ($\lambda$ = 1.54184 Å) | Cu$K_\alpha$ ($\lambda$ = 1.54184 Å) | Cu$K_\alpha$ ($\lambda$ = 1.54184 Å) | Cu$K_\alpha$ ($\lambda$ = 1.54184 Å) |
| data collection 2$\theta$ range / ° | 7.848−133.084 | 7.870−133.160 | 8.116−133.186 | 7.338−133.202 |
| index ranges | −15 ≤ $h$ ≤ 15<br>−6 ≤ $k$ ≤ 6<br>−26 ≤ $l$ ≤ 26 | −15 ≤ $h$ ≤ 15<br>−6 ≤ $k$ ≤ 7<br>−26 ≤ $l$ ≤ 26 | −9 ≤ $h$ ≤ 11<br>−12 ≤ $k$ ≤ 13<br>−14 ≤ $l$ ≤ 14 | −14 ≤ $h$ ≤ 13<br>−15 ≤ $k$ ≤ 14<br>−26 ≤ $l$ ≤ 26 |
| collected reflections | 34051 | 38576 | 11065 | 44069 |
| unique reflections | 2925 | 3009 | 4003 | 11202 |
| unique reflections [$I > 2\sigma(I)$] | 2543 [$I > 2\sigma(I)$] | 2560 [$I > 2\sigma(I)$] | 2871 [$I > 2\sigma(I)$] | 8184 [$I > 2\sigma(I)$] |
| $R_{int}$ | 0.0354 | 0.0423 | 0.0323 | 0.0385 |
| $R(F)$, $F > 2\sigma$(F) | 0.0336 | 0.0361 | 0.0777 | 0.0473 |
| $wR(F^2)$, $F > 2\sigma$(F) | 0.0826 | 0.0948 | 0.2255 | 0.1261 |
| $R(F)$, all data | 0.0391 | 0.0432 | 0.0974 | 0.0655 |
| $wR(F^2)$, all data | 0.0859 | 0.0999 | 0.2467 | 0.1345 |
| $\Delta_r$ (max., min.) e Å$^{-3}$ | 0.186/−0.238 | 0.198/−0.218 | 0.408/−0.451 | 0.359/−0.309 |
| CCDC deposition number | 2413777 | 2413778 | 2413779 | 2413780 |

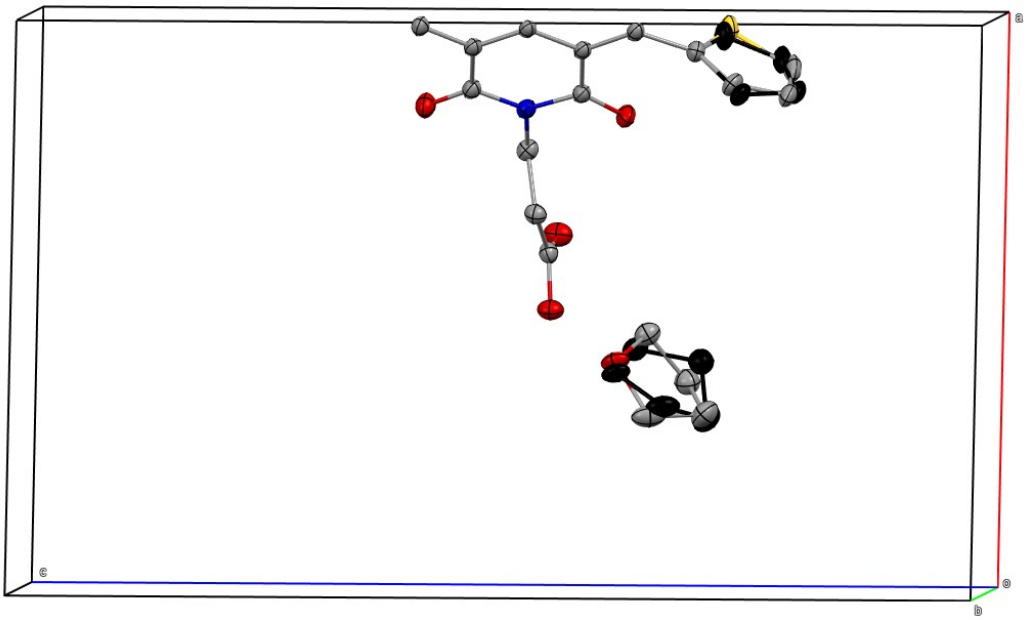

**Figure S20.** The asymmetric unit of the **NDI-Th** THF solvate. The thermal ellipsoids are drawn at the 50% probability level. The minor occupancy sites are highlighted in black. All hydrogen atoms have been omitted for clarity. Colour scheme: carbon – grey, nitrogen – blue, oxygen – red, sulfur – yellow.

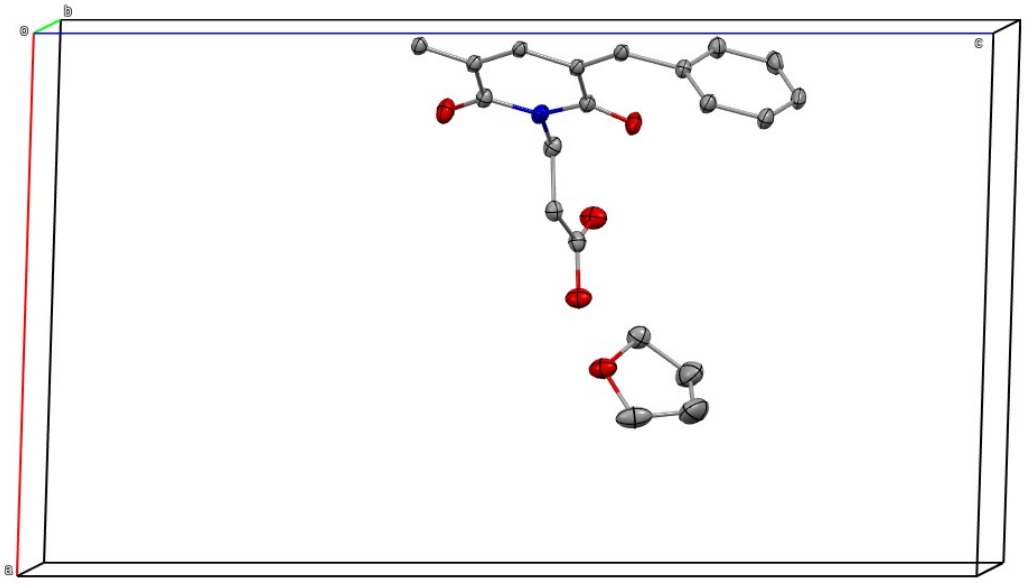

**Figure S21.** The asymmetric unit of the **NDI-Ph** THF solvate. The thermal ellipsoids are drawn at the 50% probability level. The minor occupancy sites are highlighted in black. All hydrogen atoms have been omitted for clarity. Colour scheme: carbon – grey, nitrogen – blue, oxygen – red.

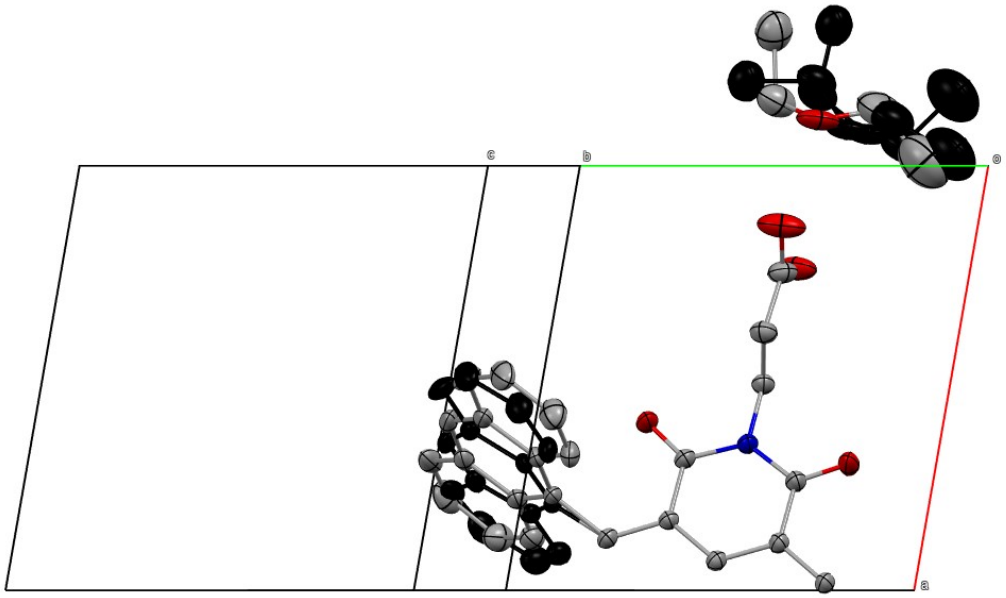

**Figure S22.** The asymmetric unit of the **NDI-An** diethyl ether solvate. The thermal ellipsoids are drawn at the 50% probability level. The minor occupancy sites are highlighted in black. All hydrogen atoms have been omitted for clarity. Colour scheme: carbon – grey, nitrogen – blue, oxygen – red.

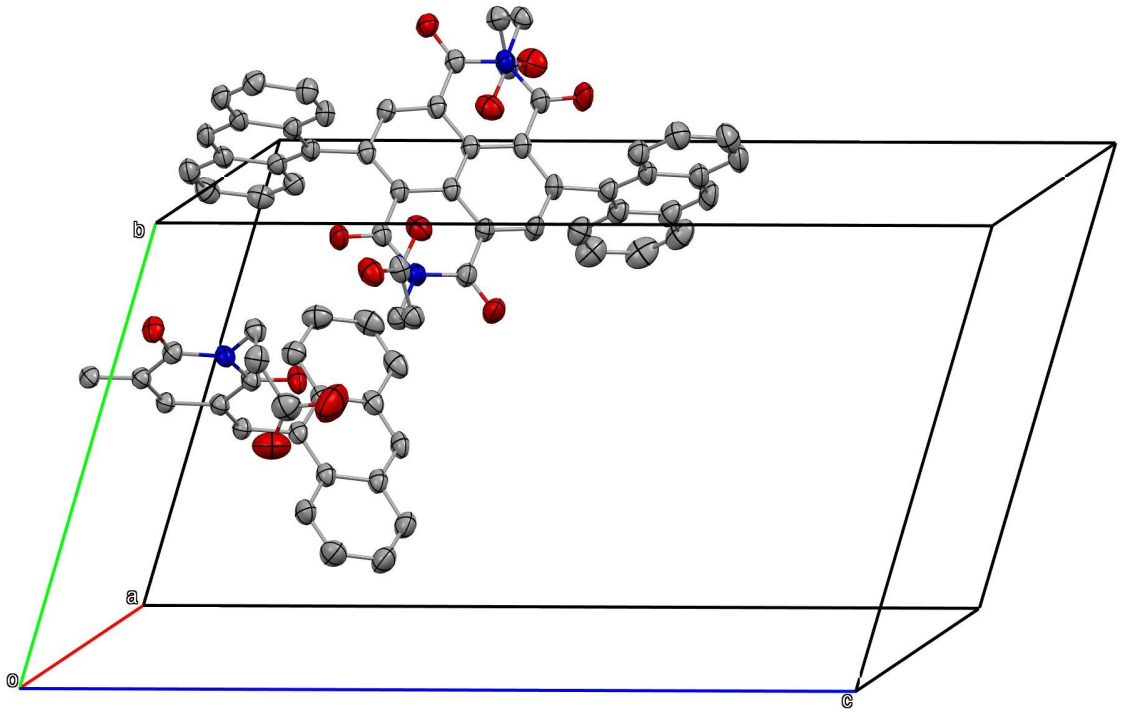

**Figure S23.** The asymmetric unit of the **NDI-An** diethyl-ether THF solvate. The thermal ellipsoids are drawn at the 50% probability level. The minor occupancy sites are highlighted in black. All hydrogen atoms have been omitted for clarity. Colour scheme: carbon – grey, nitrogen – blue, oxygen – red.

# 7. NMR Spectra

## $^{1}$H-NMR

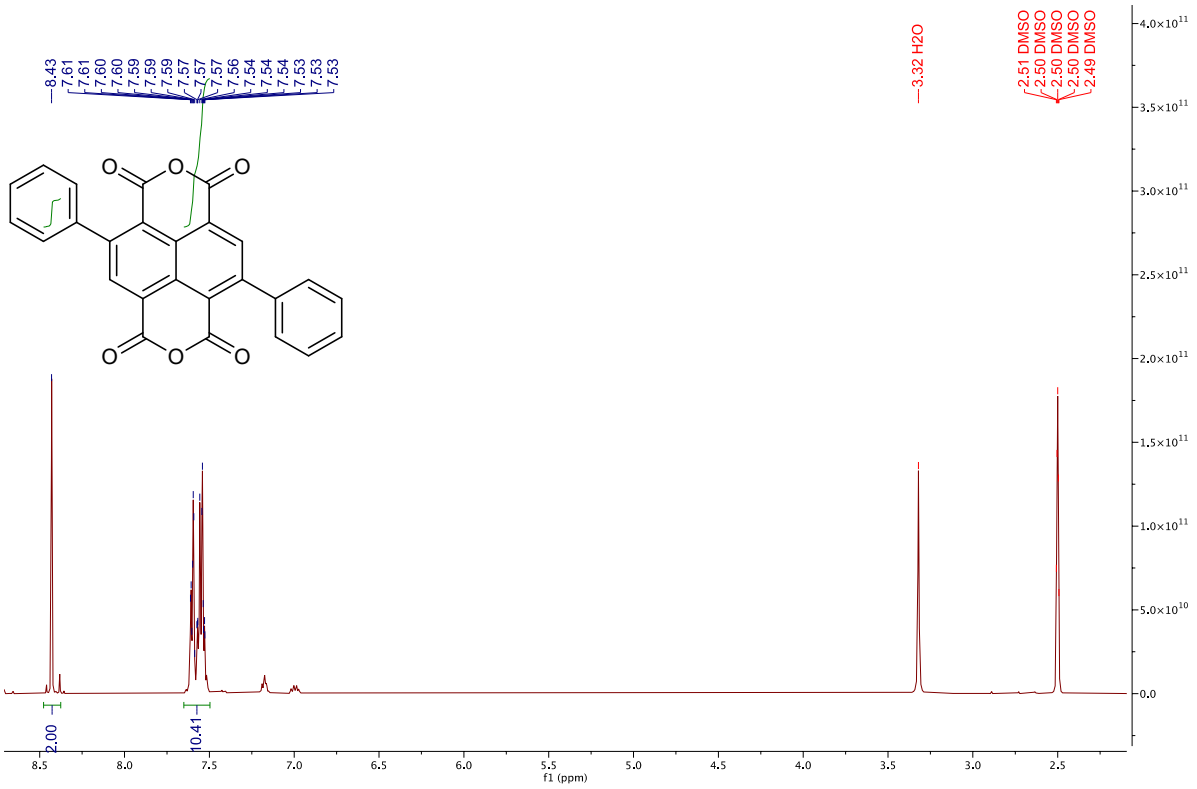


## $^{13}$C-NMR

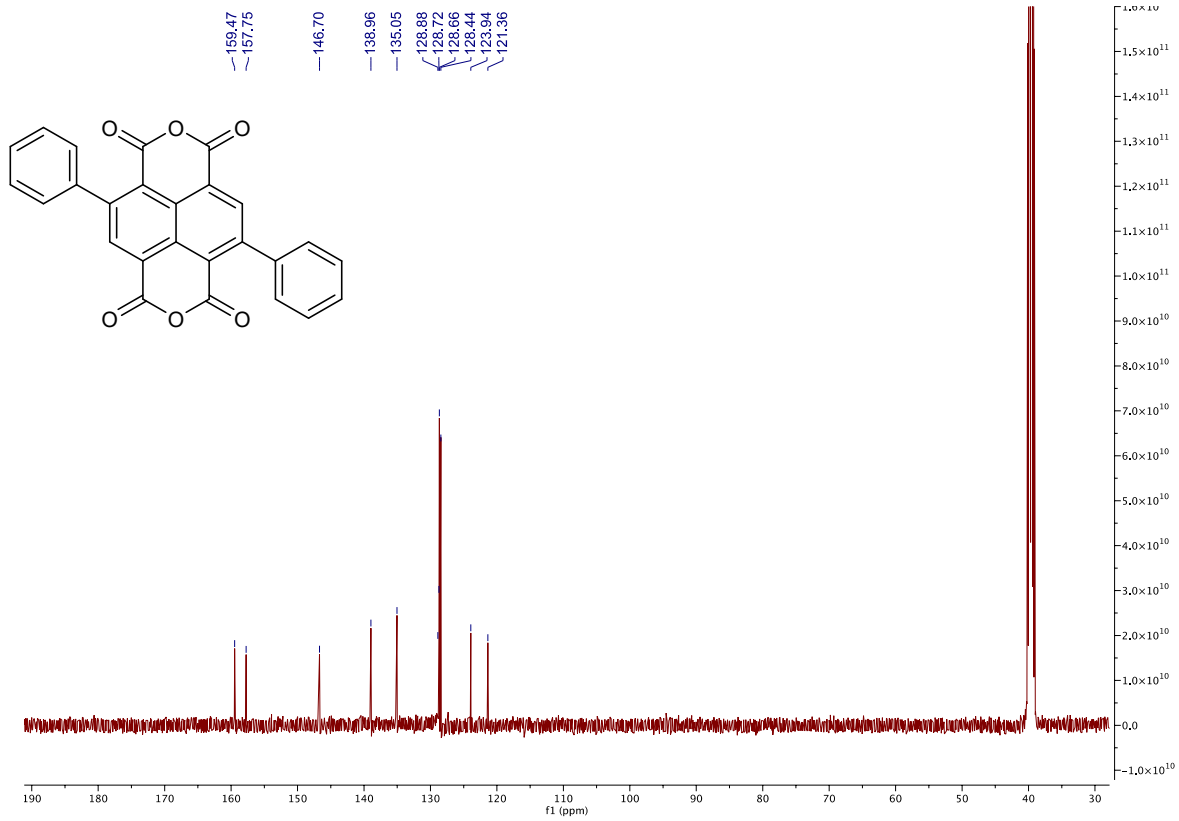

## $^{1}$H-NMR

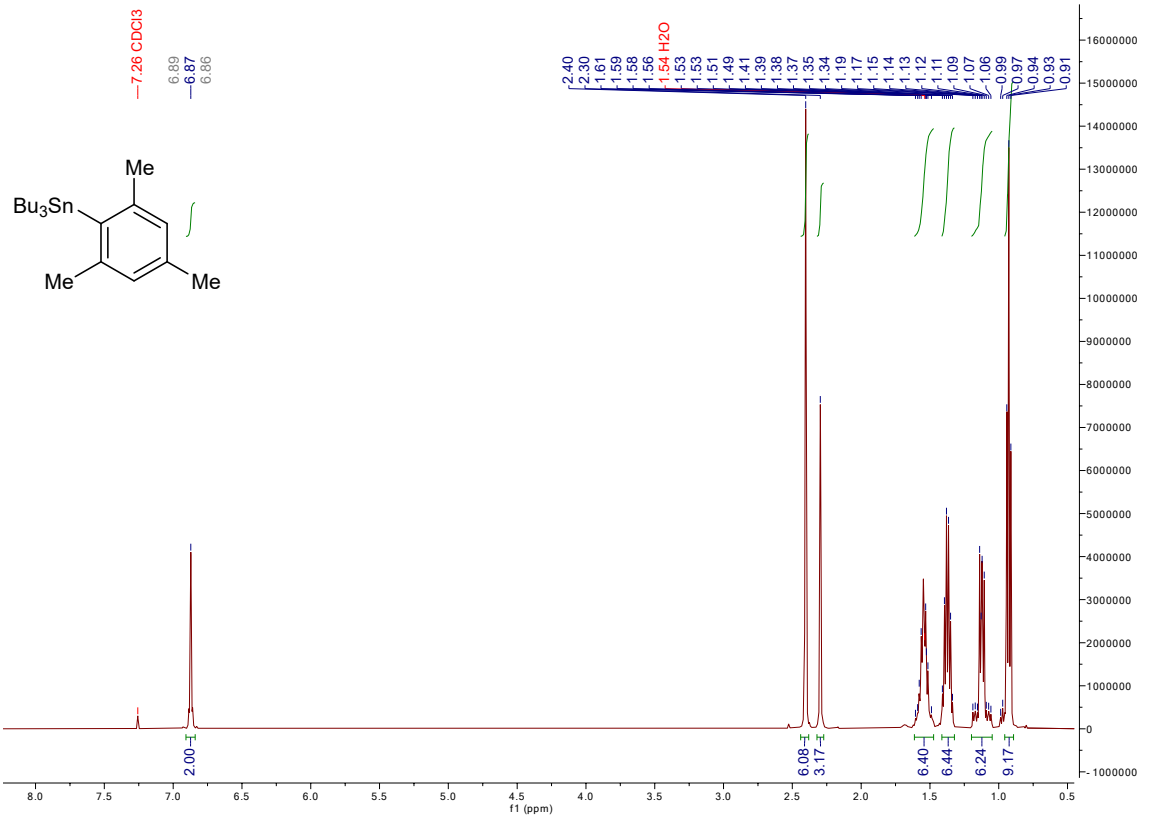


## $^{13}$C-NMR

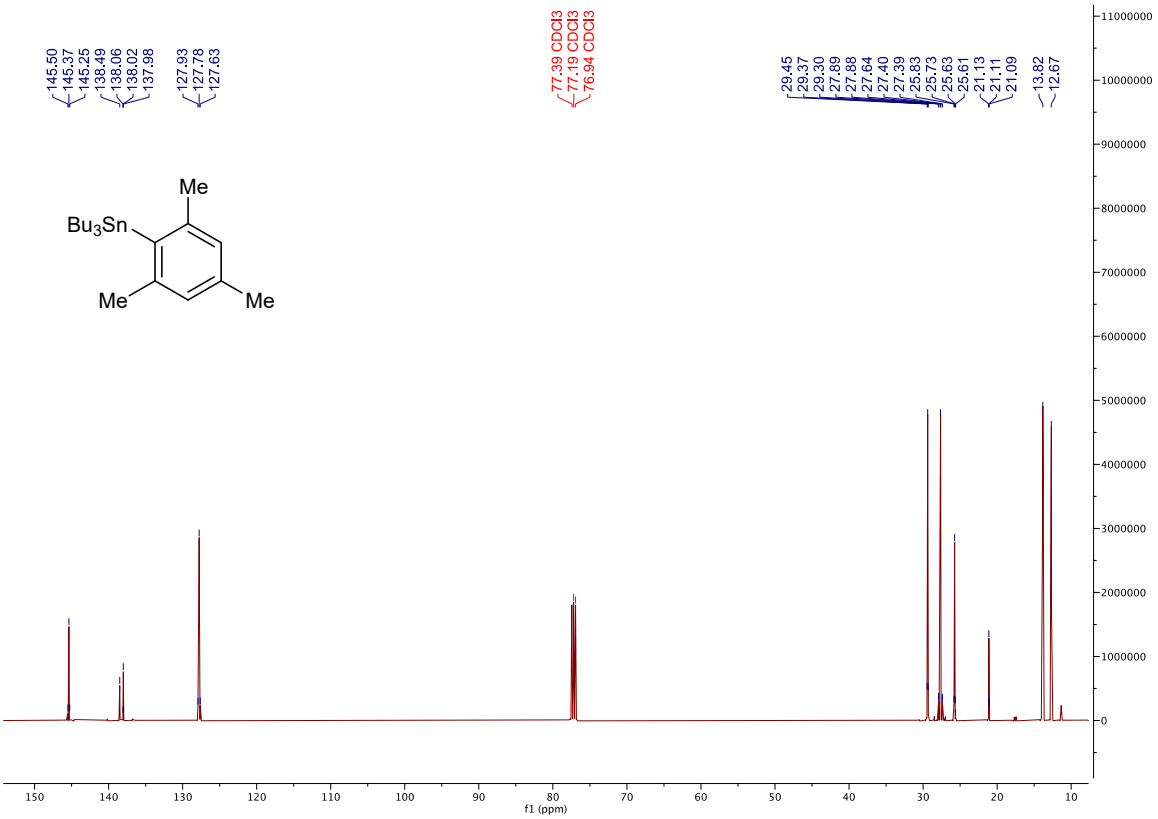

## $^{1}$H-NMR

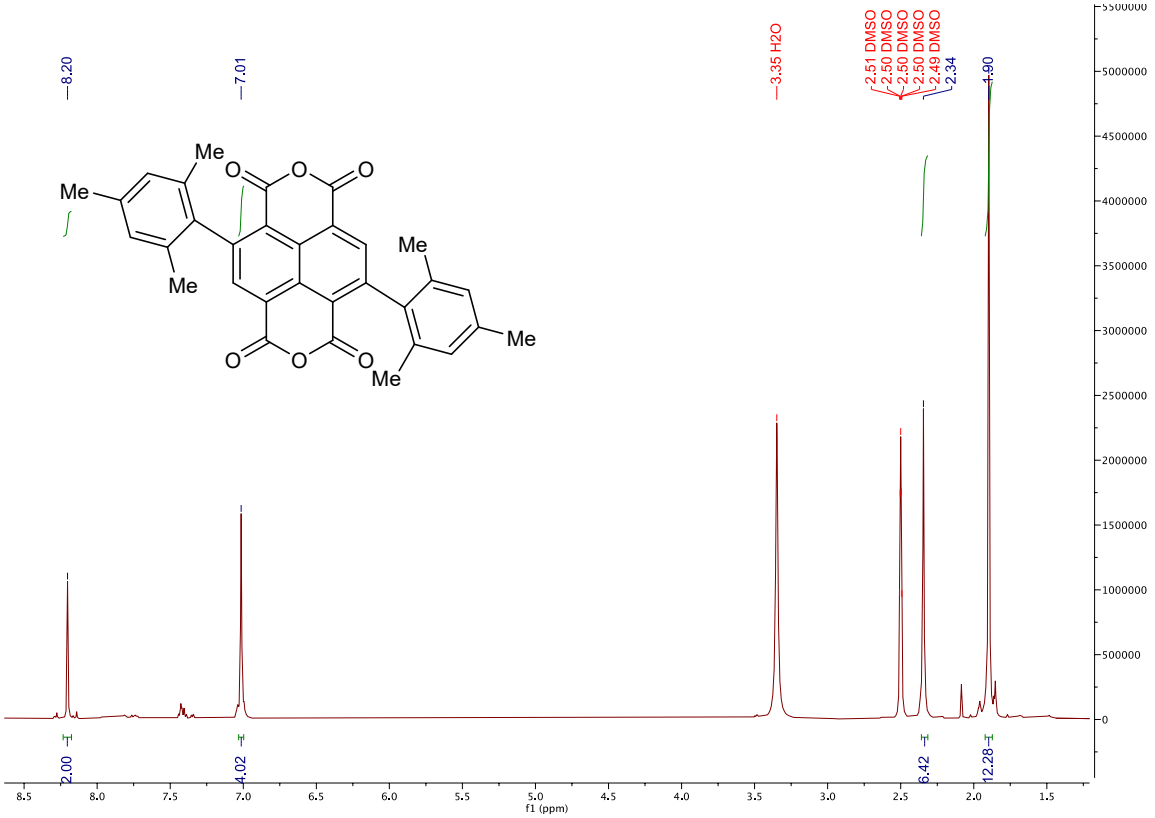


## $^{13}$C-NMR

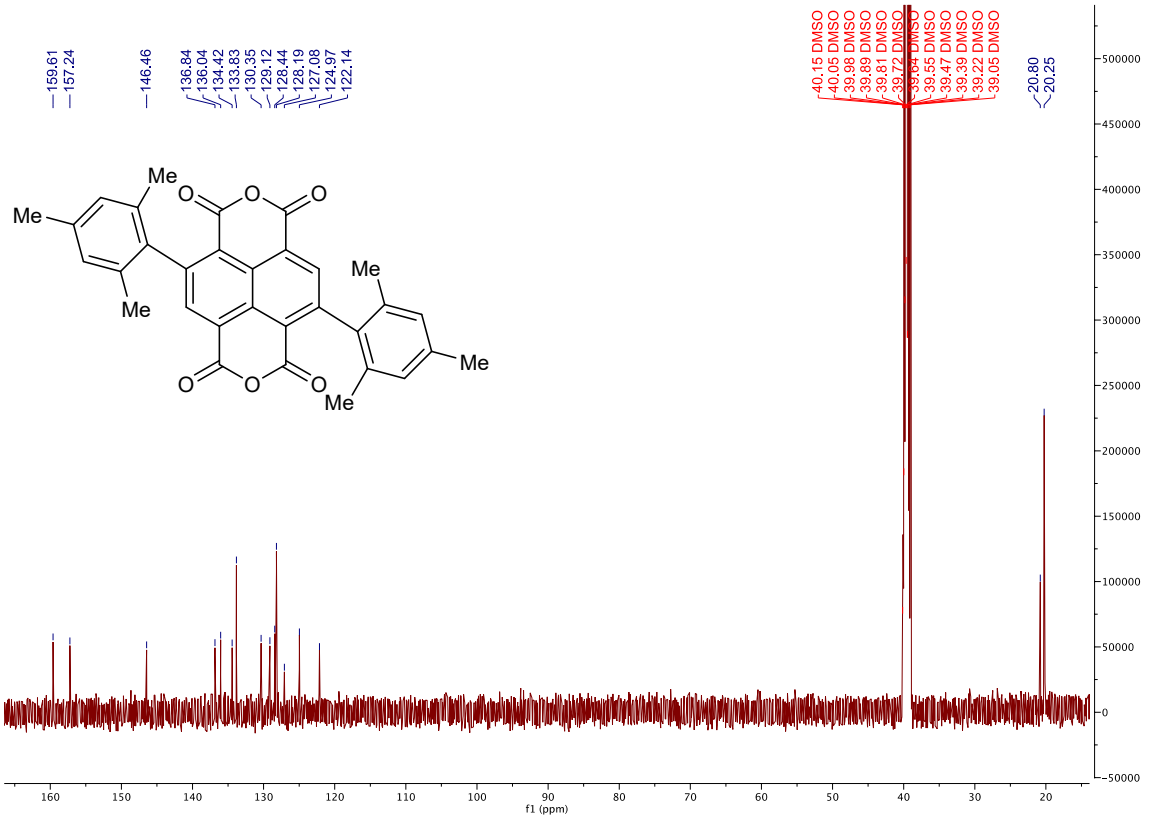

## $^{1}$H-NMR

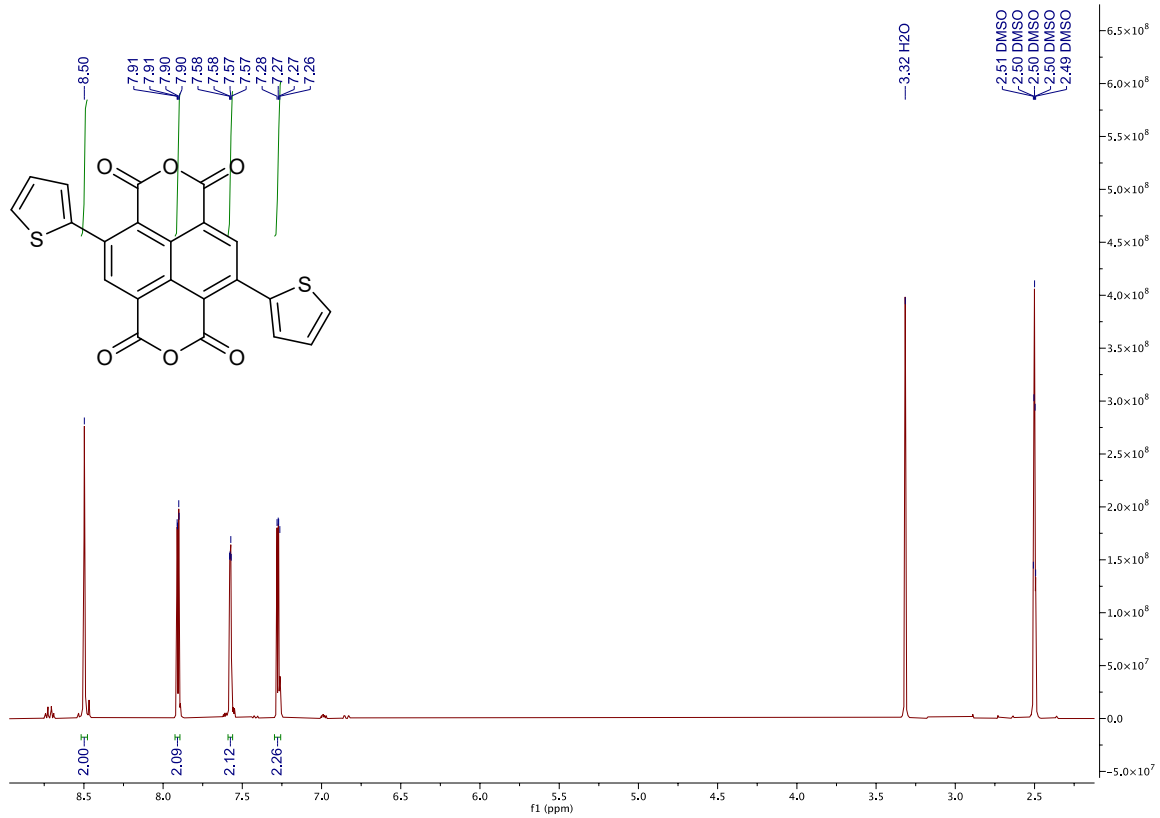


## $^{13}$C-NMR

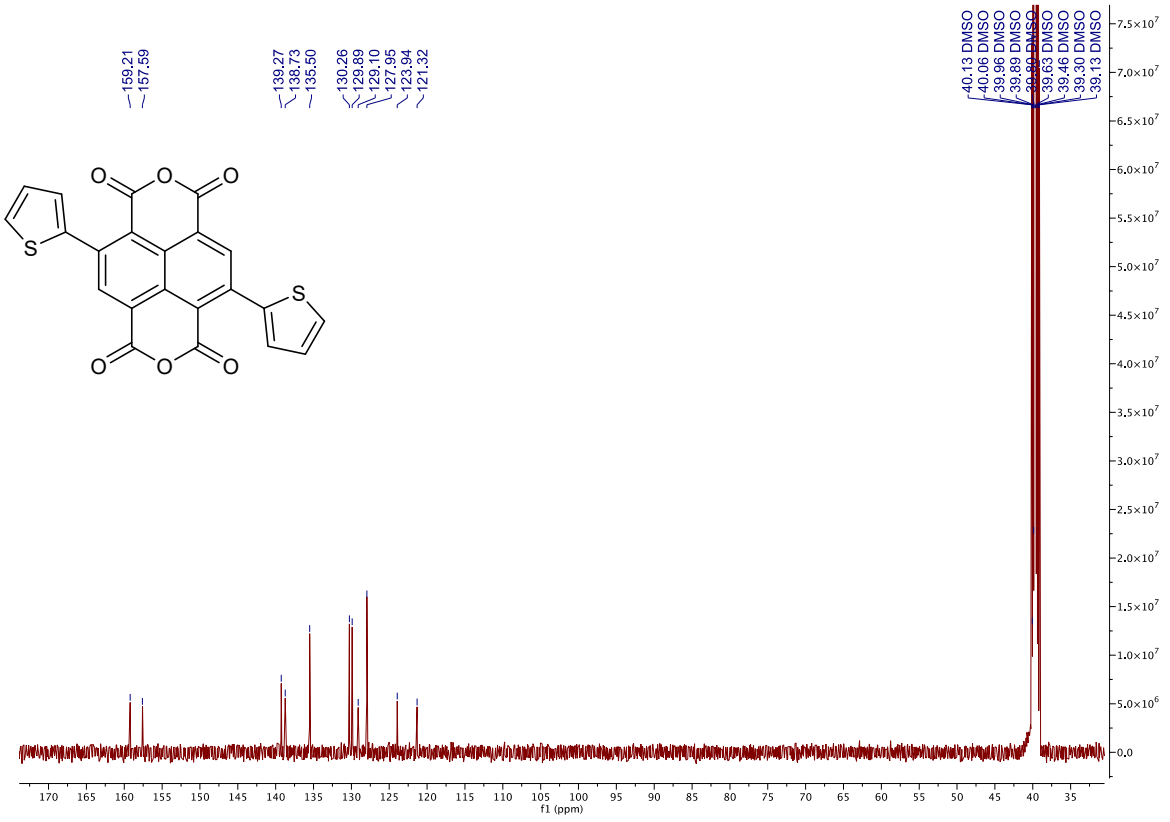

## $^{1}$H-NMR

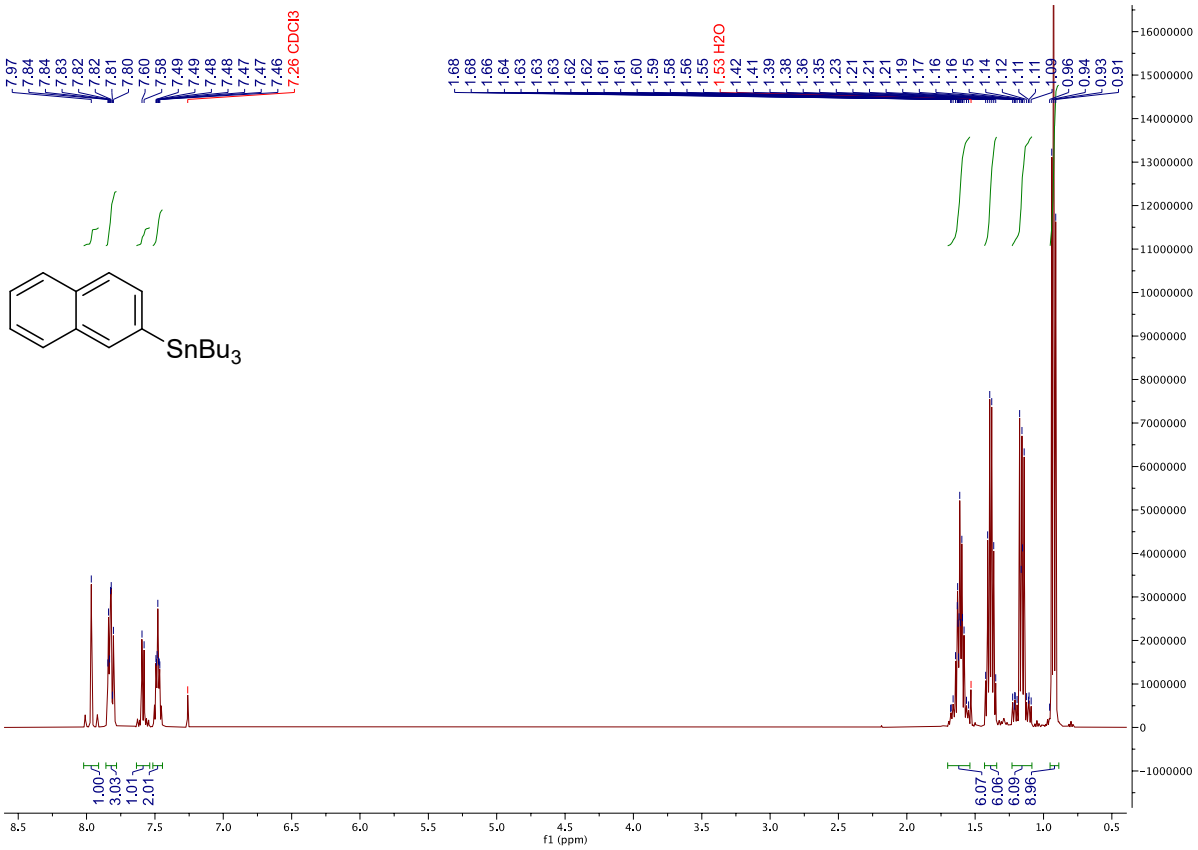


## $^{13}$C-NMR

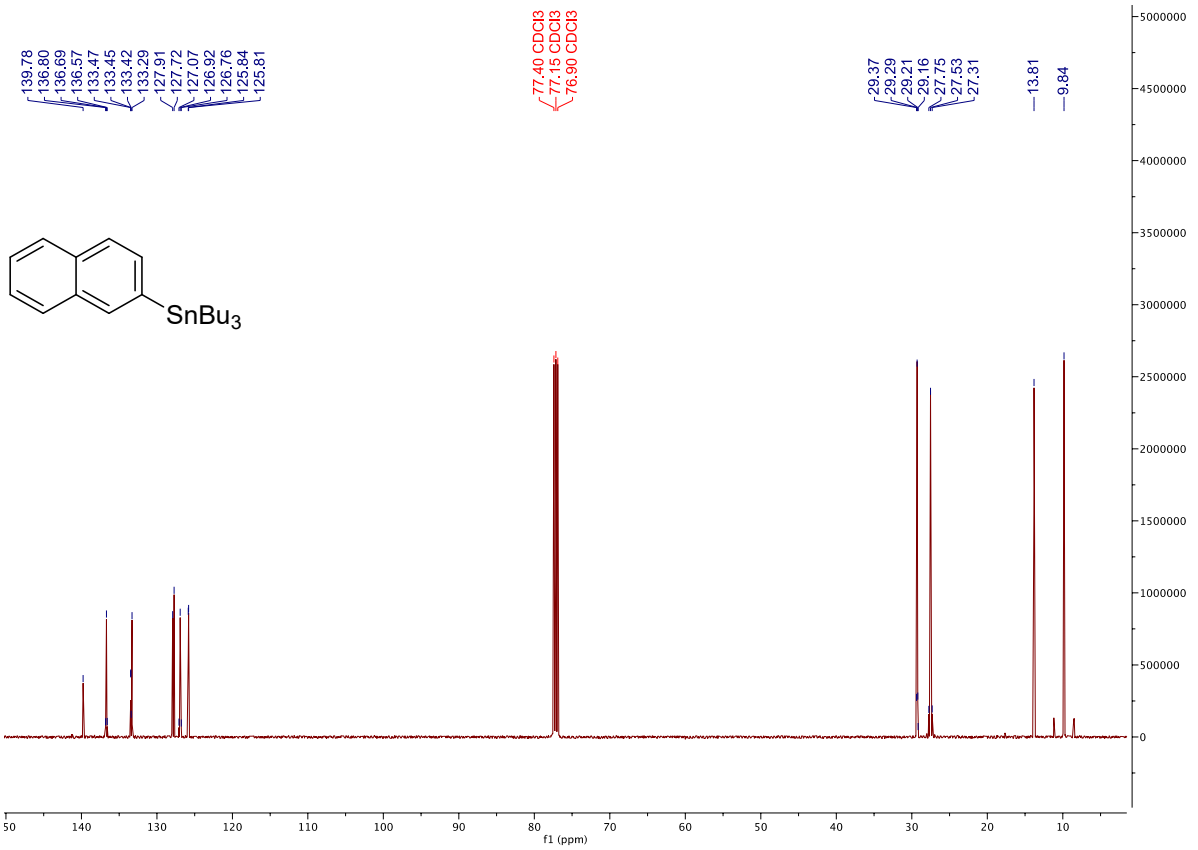

## $^{1}$H-NMR

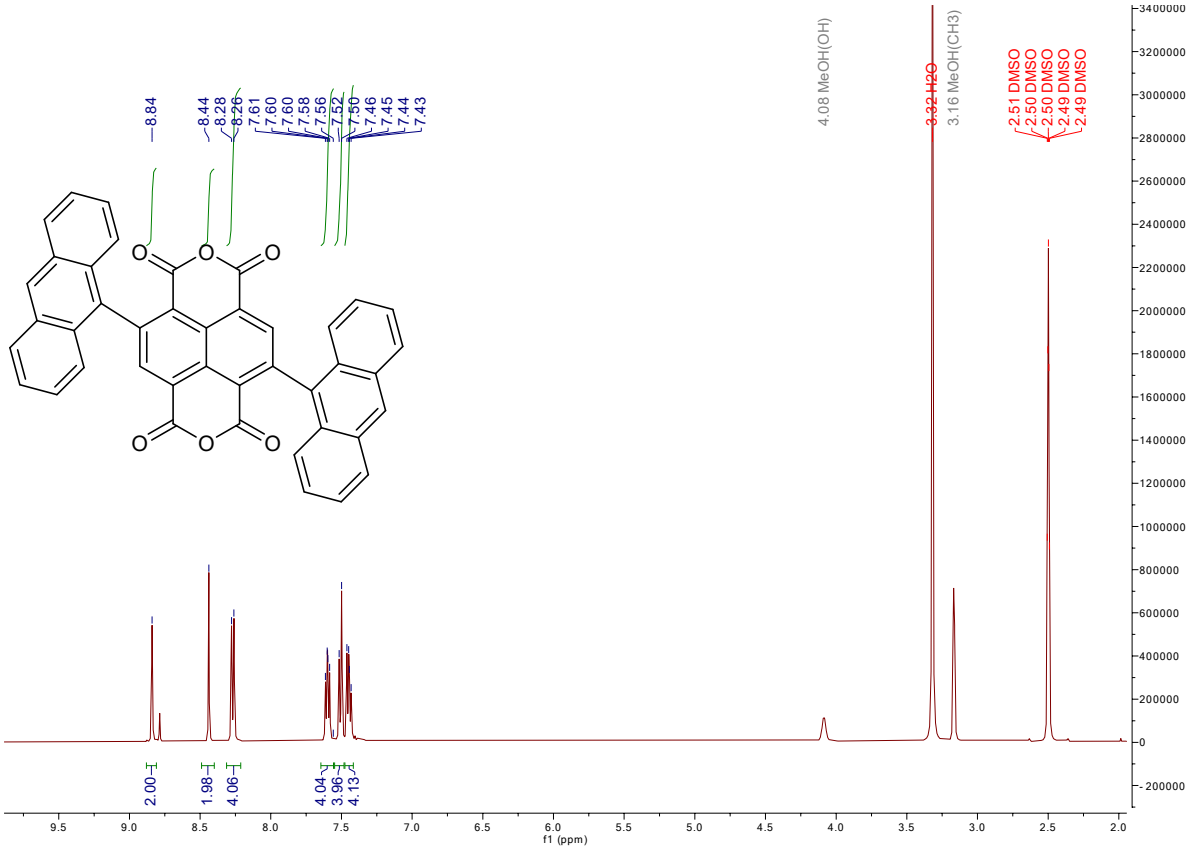


## $^{13}$C-NMR

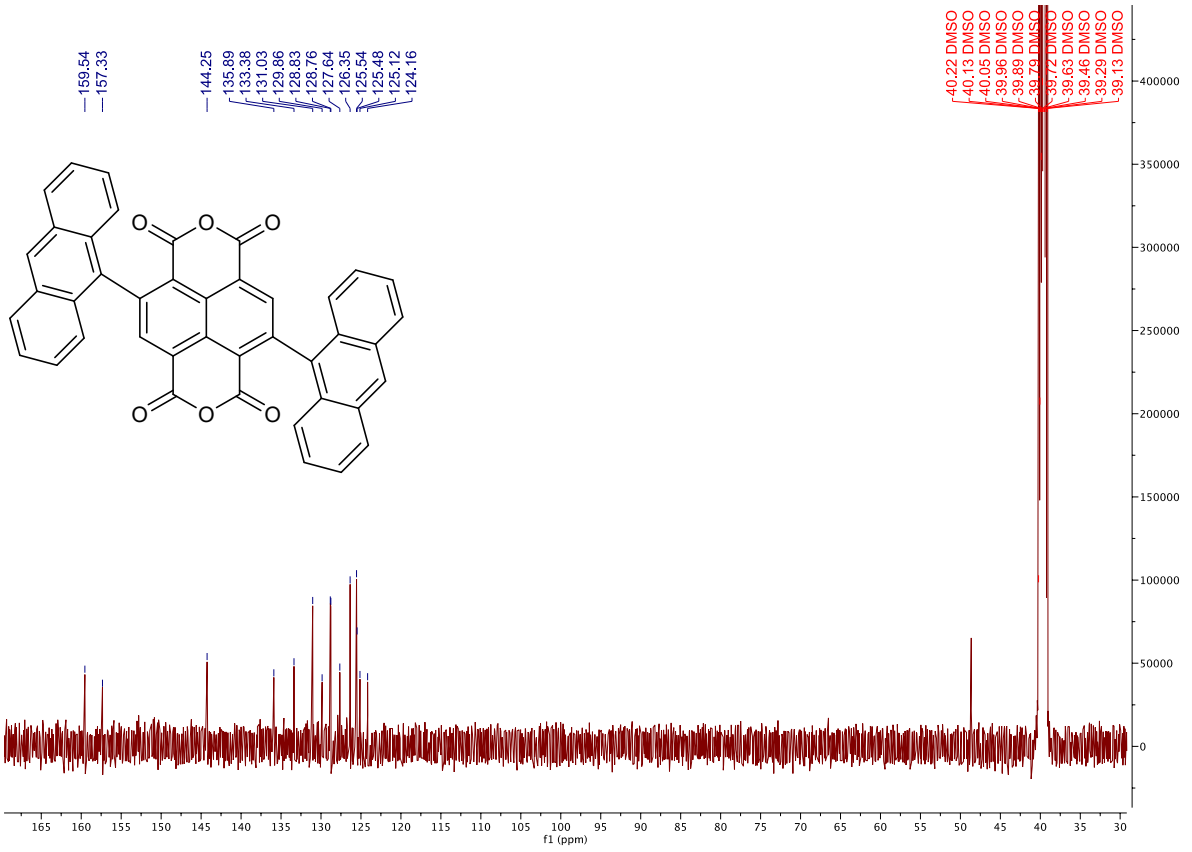

## $^{1}$H-NMR

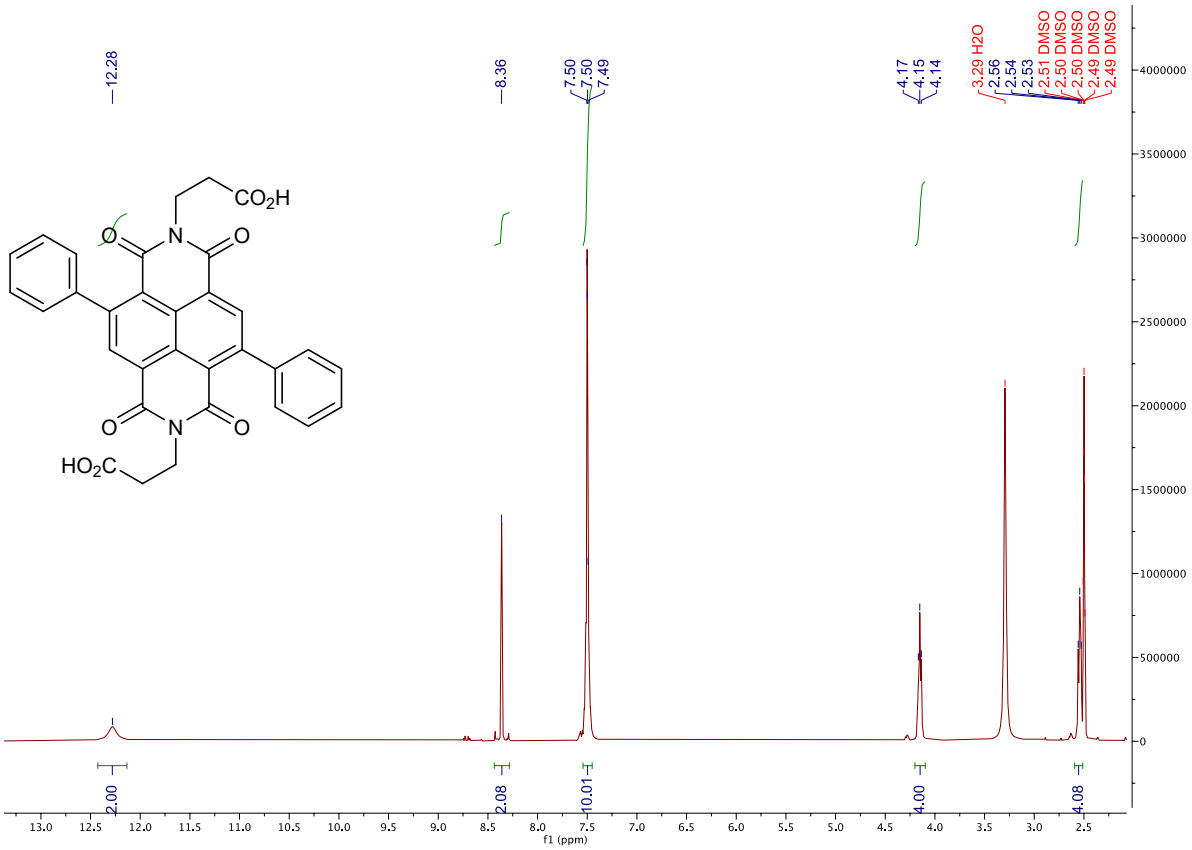


## $^{13}$C-NMR

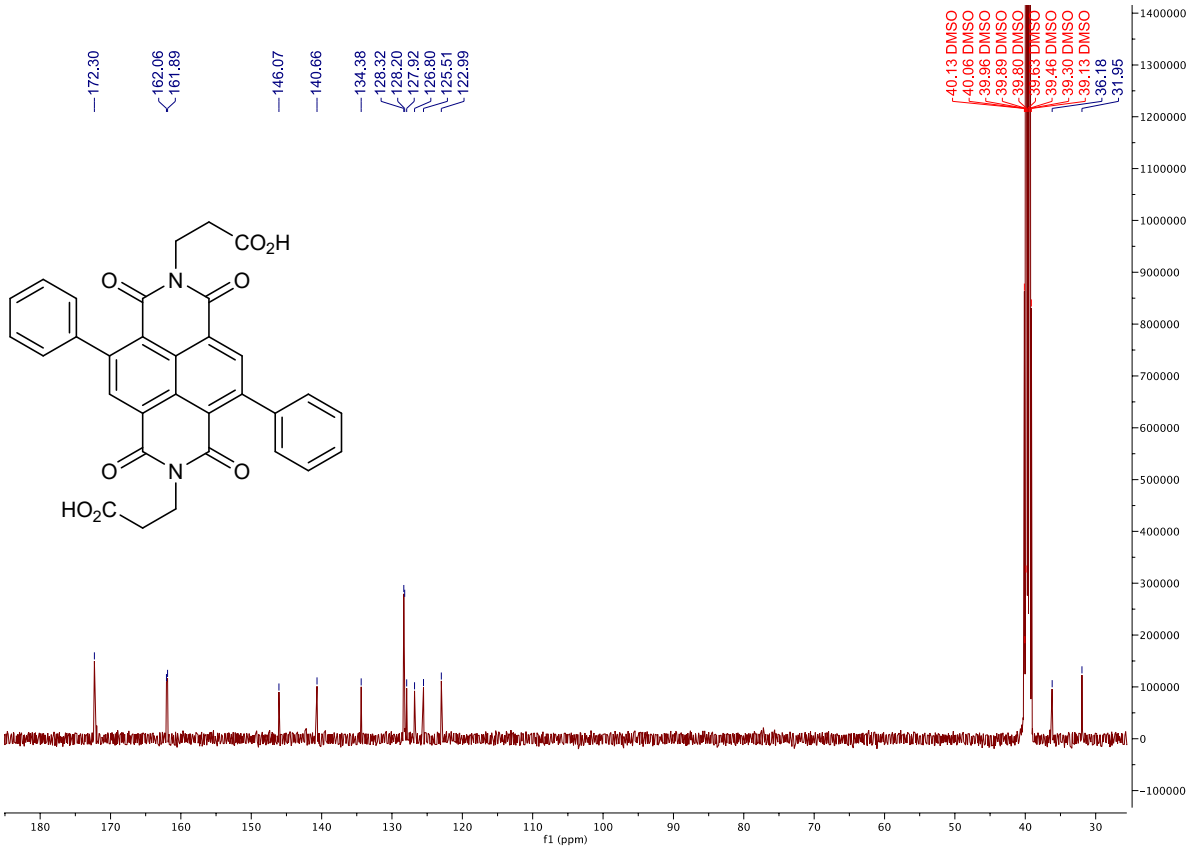

## $^{1}$H-NMR

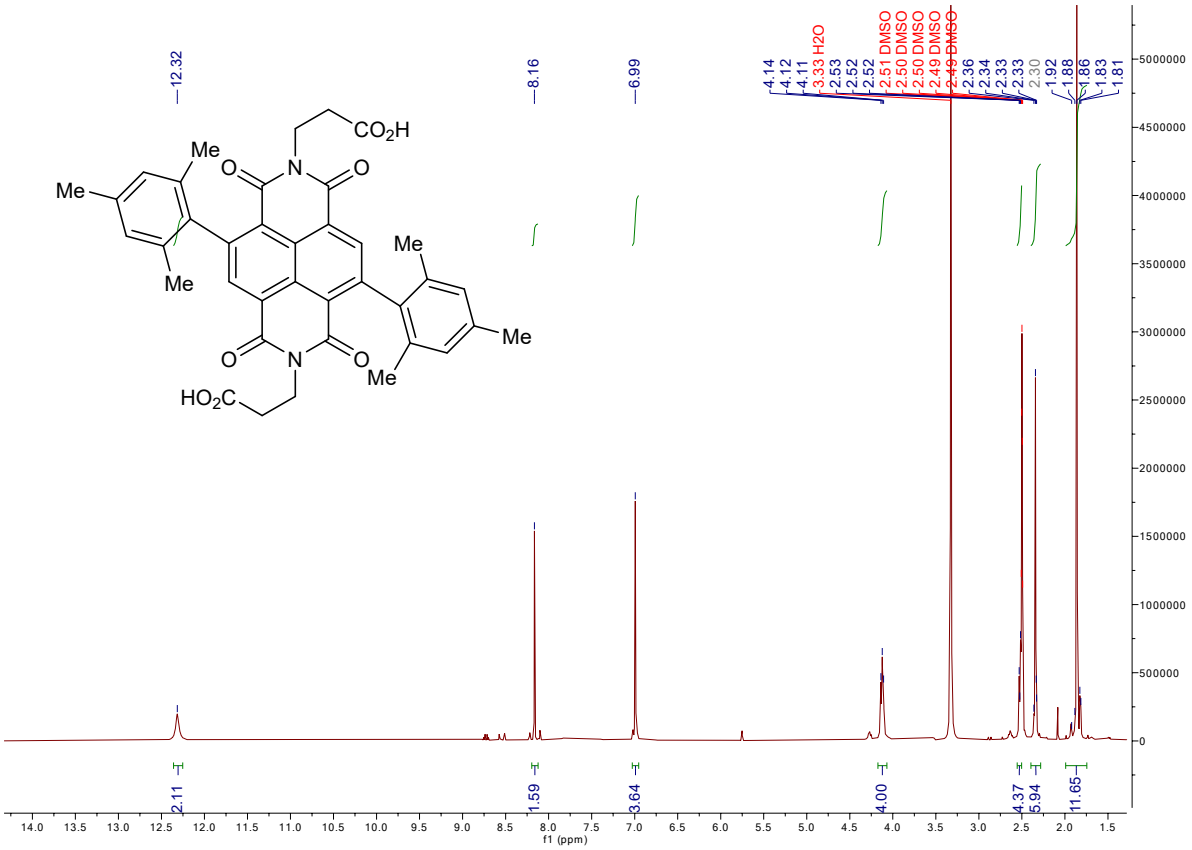


## $^{13}$C-NMR

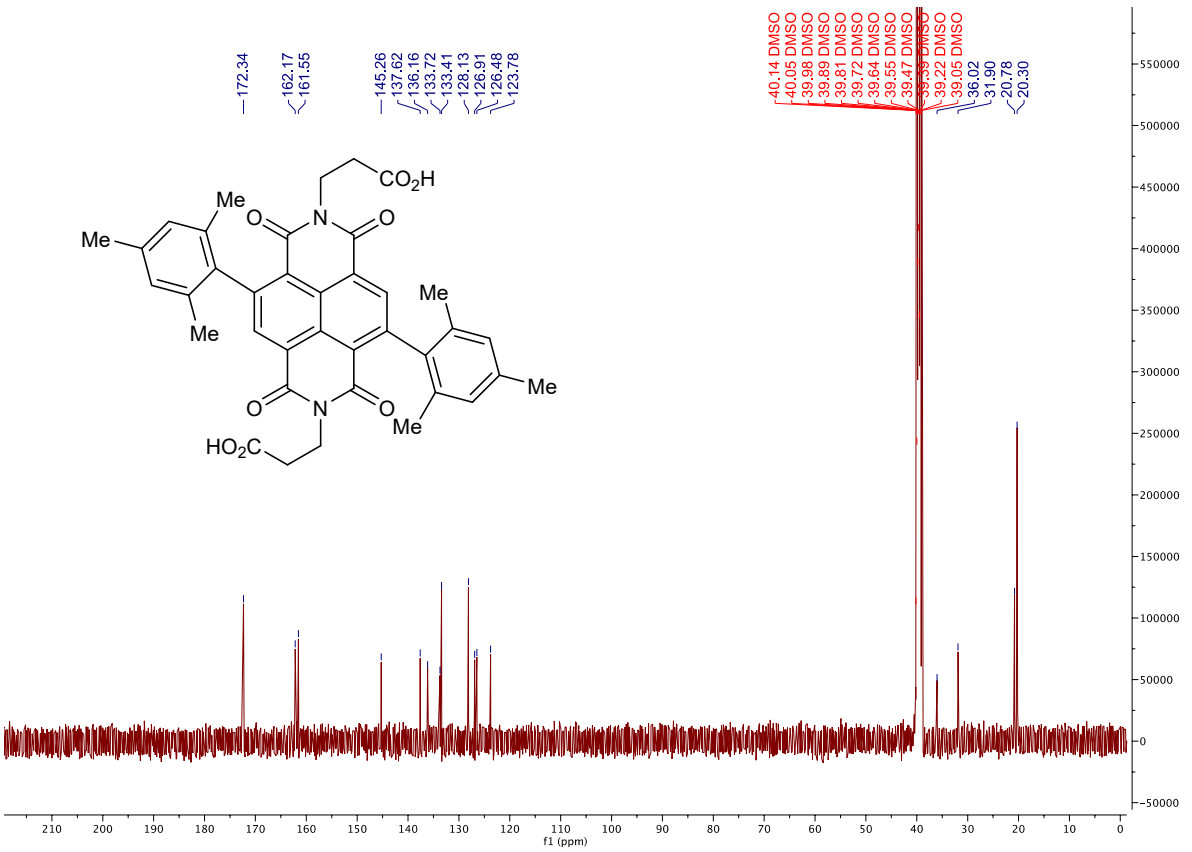

## $^{1}$H-NMR

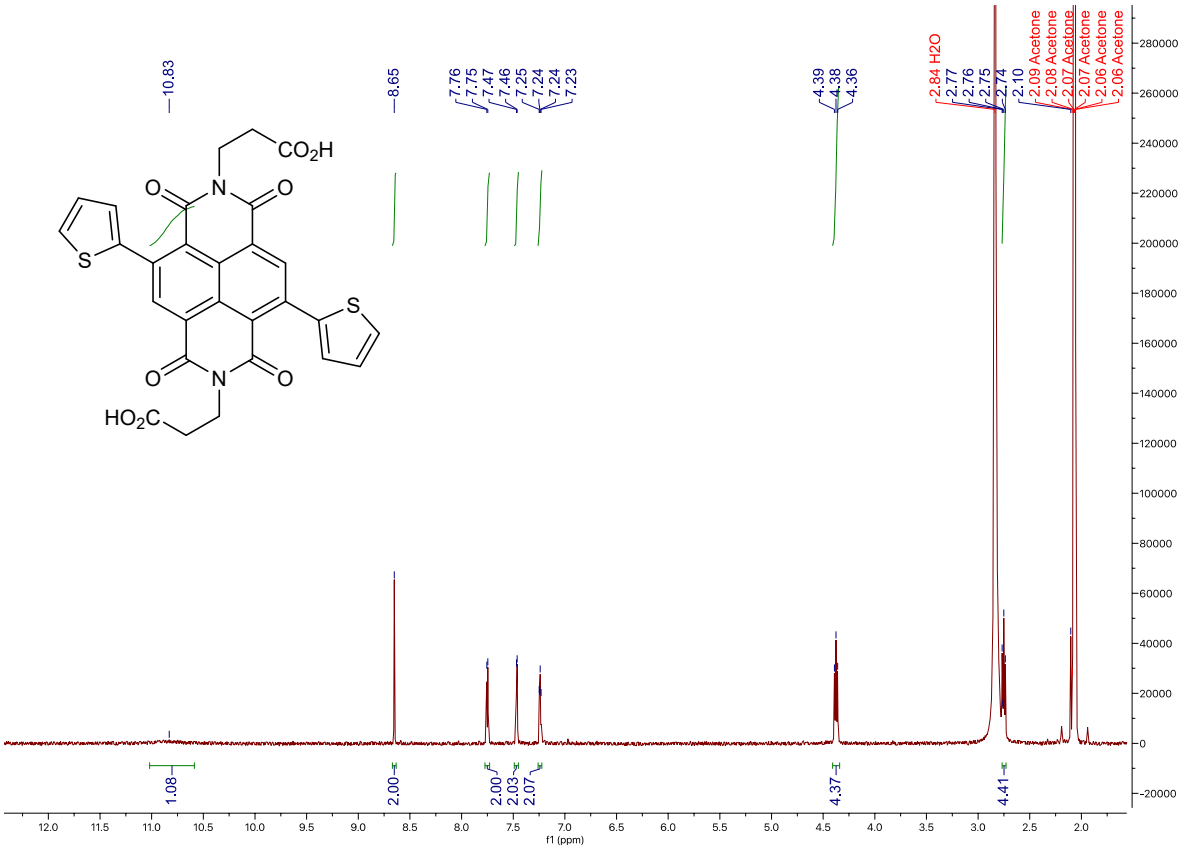


## $^{13}$C-NMR

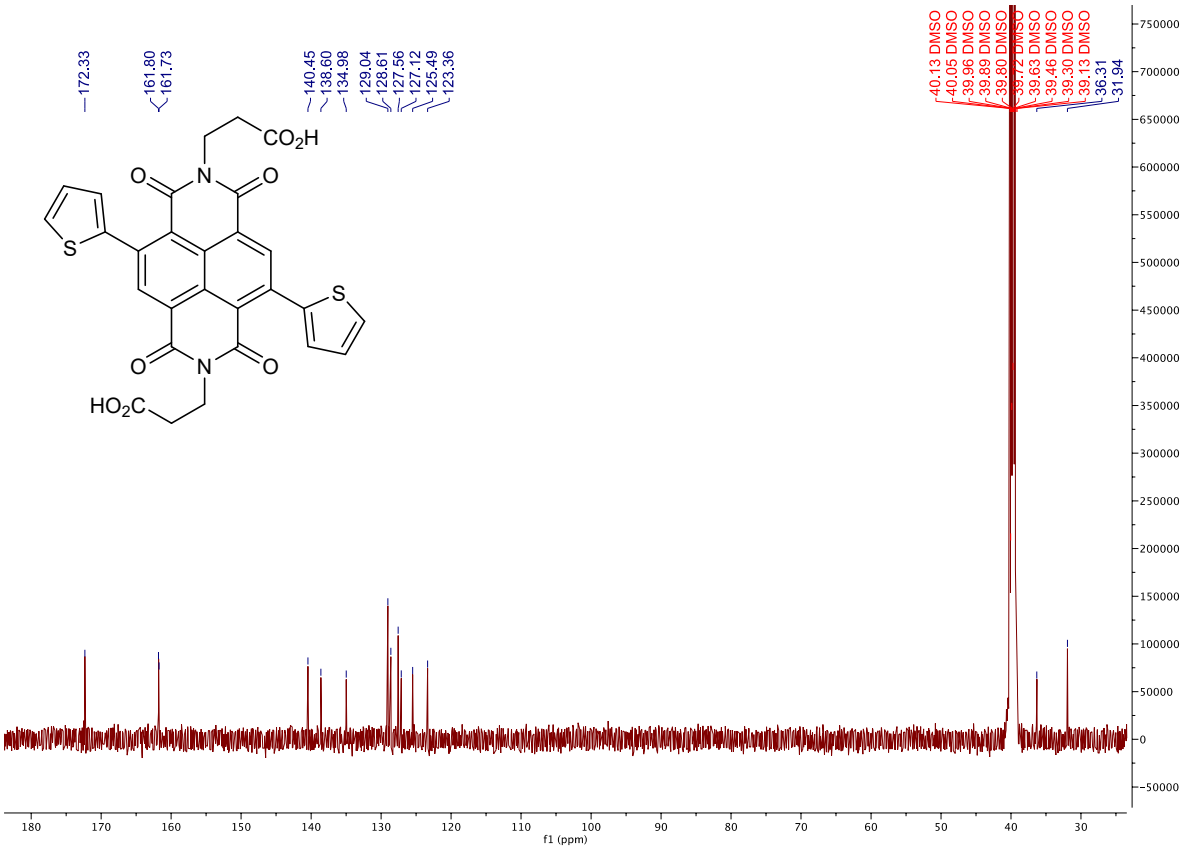

## $^{1}$H-NMR

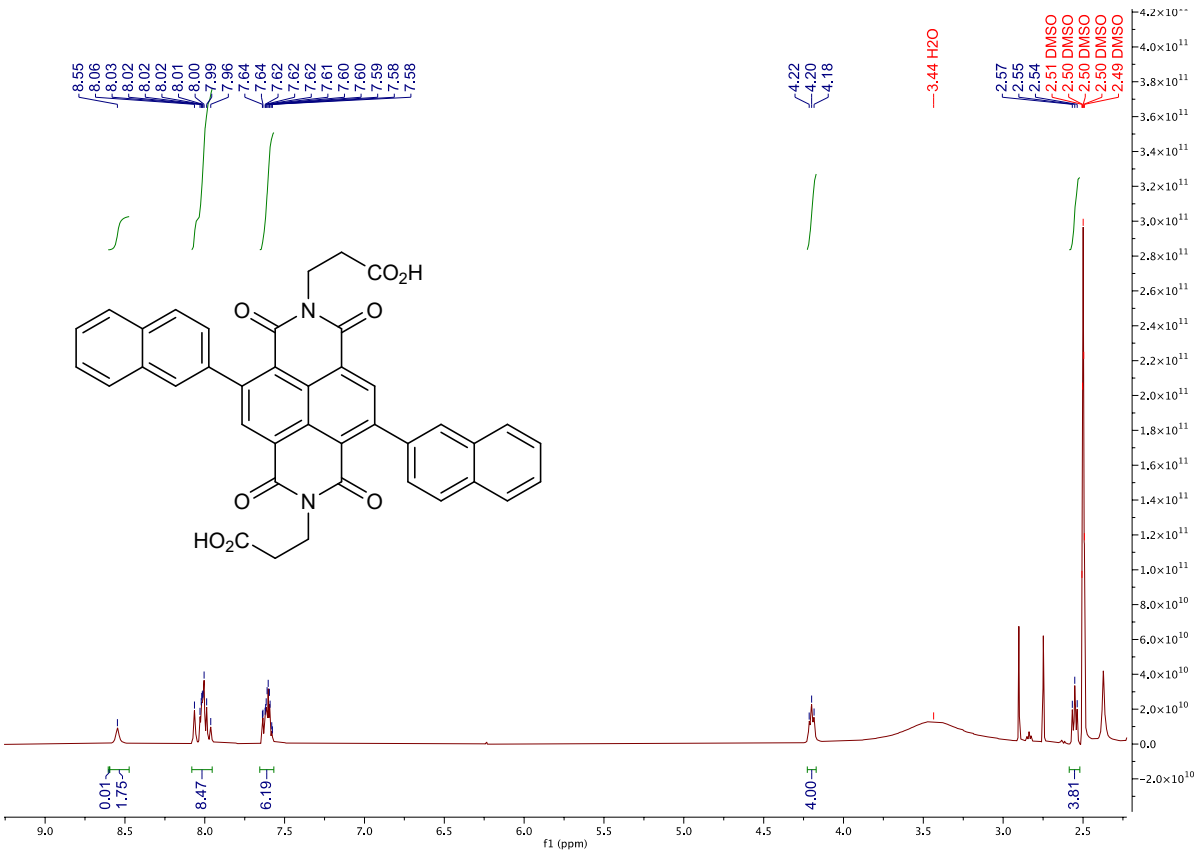


## $^{13}$C-NMR

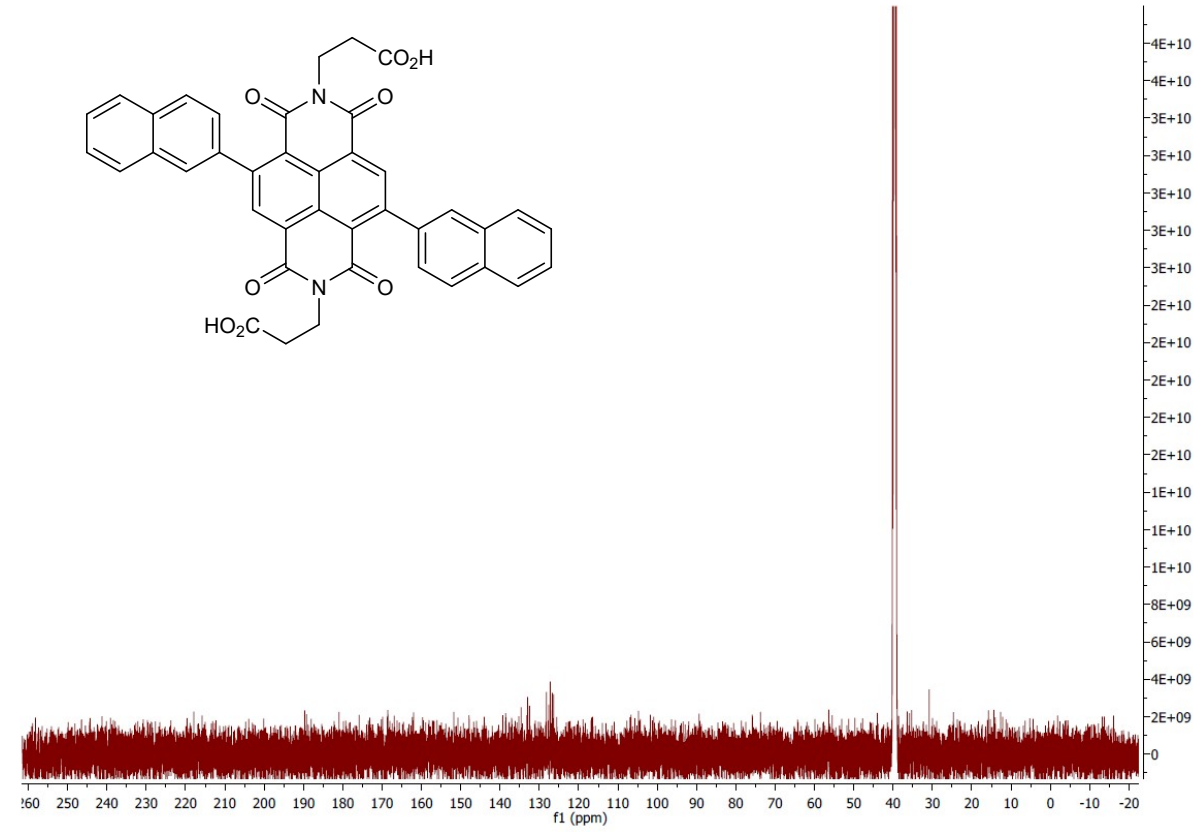

## $^{1}$H-NMR

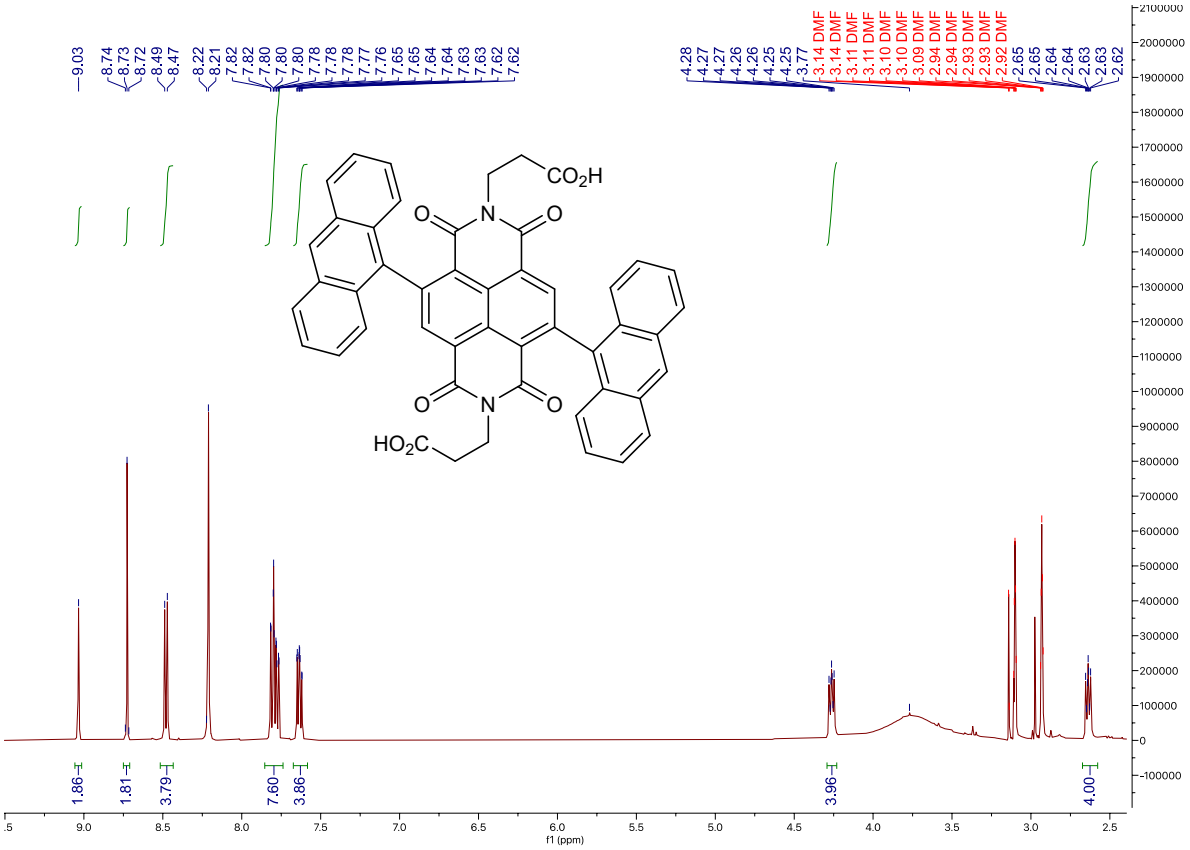


## $^{13}$C-NMR

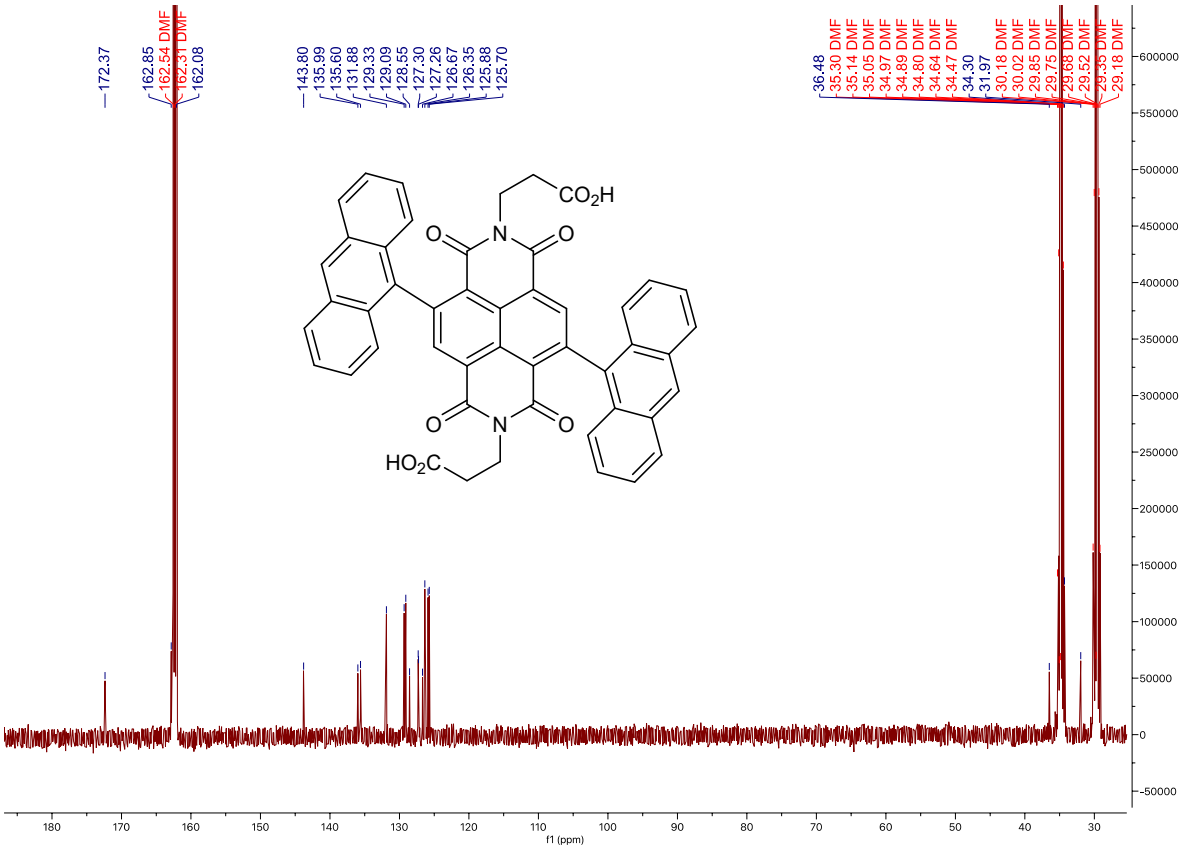

## 8. References


[1] P. Piyakulawat, A. Keawprajak, A. Chindaduang, M. Hanusch, U. Asawapirom, *Synth. Met.,* **2009**, *159*, 467–472.

[2] J. Royakkers, K. Guo, D. T. W. Toolan, L. Feng, A. Minotto, D. G. Congrave, M. Danowska, W. Zeng, A. D. Bond, M. Al-Hashimi, T. J. Marks, A. Facchetti, F. Cacialli, H. Bronstein, *Angew. Chem. Int. Ed.,* **2021**, *60*, 25005–25012.

[3] A. C. Thompson, H. M. Grimm, A. Gray Bé, K. J. McKnight, J. J. Reczek, *Synth. Commun.,* **2015**, *45*, 1127–1136.

[4] A. Sarkar, T. Behera, R. Sasmal, R. Capelli, C. Empereur-mot, J. Mahato, S. S. Agasti, G. M. Pavan, A. Chowdhury, S. J. George, *J. Am. Chem. Soc.,* **2020**, *142*, 11528–11539.

[5] CrysAllisPro 1.171.42.60a, Rigaku, **2022**.

[6] G. M. Sheldrick, *Acta Crystallogr. A Found Adv* **2015**, *64*, 3–8.

[7] O. V. Dolomanov, L. J. Bourhis, R. J. Gildea, J. A. K. Howard, H. Puschmann, *J. Appl. Crystallogr.,* **2009**, *42*, 339–341.

[8] G. M. Sheldrick, *Acta Crystallogr. Section C* **2015**, *71*, 3–8.

[9] C. B. Hübschle, G. M. Sheldrick, B. Dittrich, *J. Appl. Crystallogr.* **2011**, *44*, 1281–1284.

[10] B. Rees, L. Jenner, M. Yusupov, *Acta Crystallogr. D. Biol. Crystallogr.* **2005**, *61*, 1299–1301.

[11] Y. Yu, J. Wang, Y. Cui, Z. Chen, T. Zhang, Y. Xiao, W. Wang, J. Wang, X.-T. Hao, J. Hou, *J Am Chem Soc* **2024**, *146*, 8697–8705.

[12] P. Tang, T. Furuya, T. Ritter, *J. Am. Chem. Soc.,* **2010**, *132*, 12150–12154.

[13] Y. Chen, M. Chen, Y. Liu, *Angew. Chem. Int. Ed.,* **2012**, *51*, 6181–6186.

[14] N. N. Sergeeva, A. Scala, M. A. Bakar, G. O'Riordan, J. O'Brien, G. Grassi, M. O. Senge, *J. Org. Chem.,* **2009**, *74*, 7140–7147.

[15] M. Fujitsuka, S. S. Kim, C. Lu, S. Tojo, T. Majima, *J. Phys. Chem. B*, **2015**, *119*, 24, 7275–7282.